**Functional characterization of the Met50Val substitution in *SLC30A9* as a novel case of adaptive introgression in humans**

Ana Roca-Umbert[1], Marina Vogel-González[2], Alejandro Fierro-Villegas[2], Jorge García-Calleja[1], Anja Bosnjak[2], Gerard Ill-Raga[2], Víctor Herrera-Fernández[2], Gerard Muntané[1,3,4], Felix Campelo[5], Rubén Vicente[2 *], Elena Bosch[1,4 *]

[1]Institut de Biologia Evolutiva (UPF-CSIC), Departament de Medicina i Ciències de la Vida, Universitat Pompeu Fabra, Parc de Recerca Biomèdica de Barcelona, Doctor Aiguader 88, 08003 Barcelona, Spain

[2]Laboratory of Molecular Physiology, Department of Medical and Life Sciences, Universitat Pompeu Fabra, 08003 Barcelona, Spain

[3]Hospital Universitari Institut Pere Mata, IISPV, Universitat Rovira i Virgili, Reus, Spain.

[4]Centro de Investigación Biomédica en Red de Salud Mental (CIBERSAM), 43206 Reus, Spain

[5]ICFO-Institut de Ciències Fotòniques, The Barcelona Institute of Science and Technology, 08860 Barcelona, Spain

*Corresponding authors
E-mail: elena.bosch@upf.edu
E-mail: ruben.vicente@upf.edu

**Abstract**

The *SLC30A9* gene encodes a ubiquitously expressed zinc transporter (ZnT9) and has been consistently suggested as a candidate for positive selection in humans. Here, we first validated the extreme signatures of adaptation found in the *SLC30A9* region using evolutionary statistics based on population differentiation, extended haplotype homozygosity, and an excess of derived alleles. We then inferred the allelic trajectories and selection coefficients of two putative adaptive variants and tried to functionally validate their potential systemic and molecular adaptive phenotypes. Our results provide evidence for directional selection operating in two contrasting haplotypes extremely frequent in Africa and East Asia, respectively, which are not only associated with differential *SLC30A9* expression levels but differ in a methionine-to-valine substitution (Met50Val; rs1047626) in ZnT9, which was likely adaptively introgressed from archaic humans. Although we found no significant differences in systemic zinc content between individuals with different rs1047626 genotypes, we demonstrate that the overexpression of the derived isoform (ZnT9 50Val) in HEK293 cells shows a gain of function when compared with the ancestral (ZnT9 50Met) variant. Furthermore, the overexpression of the ZnT9 50Val variant avoids zinc overload in the endoplasmic reticulum and mitochondria, with an impact on cell viability and zinc toxicity. Overall, our results show that the derived ZnT9 50Val variant, which is prevalent in East Asians and found at intermediate-high frequencies in other non-African populations, is associated with functional differences in zinc handling by the mitochondria and endoplasmic reticulum, key organelles involved in cell fate and metabolism. Given the essential role of zinc in glutamatergic neurotransmission, we speculate that archaic adaptation to excitotoxicity may have driven this selection event in modern humans, while also impacting prosocial behavior and susceptibility to neuropsychiatric disorders.

## Introduction

How adaptation has shaped current genetic diversity in human populations is a long-standing question in evolutionary genetics. In turn, it has been shown that the identification and functional deciphering of adaptive variants in our genome can reveal biologically relevant variation with important phenotypic consequences in current populations (*1*, *2*). Recent access to whole-genome sequencing data from diverse human populations coupled with improvements in methods that detect the molecular signatures of natural selection in the genome have facilitated the identification of hundreds of candidate genes for positive selection in humans (*3*). As a result, several candidate regions for selection have been successfully associated with diverse adaptive phenotypes and their corresponding selective pressures, which were mostly related to our diet, immune response, high altitude environment, and UV radiation (*1*, *4*, *5*). However, our understanding of the adaptive phenotypes and functional variants underlying most of the signatures of positive selection in the human genome is still very limited.

Zinc is an essential micronutrient with different structural, catalytic, and regulatory roles in the human body (*6–8*). As adequate zinc levels are fundamental for maintaining good health, the systemic and cellular homeostasis of zinc must be tightly regulated. The proteins controlling the import and export of zinc across cell membranes are known as Zinc Transporters (ZT) (*7*, *9*). The 24 ZTs identified in humans can be classified in two families: the ZIP family, whose members import zinc into the cytosol, and the ZnT family, whose function is to export zinc outside the cell or into the cell organelles. The 14 ZIP transporters are encoded by the *SLC39A1-14* genes, whereas the 10 ZnT transporters are encoded by the *SLC30A1-10* genes (*7*, *10–12*). Variation in this set of 24 ZT encoding genes can lead to zinc dysregulation at a cellular or systemic level, and given the fundamental role of zinc in the human organism, such zinc imbalance might cause alterations in distinct phenotypes upon which adaptive selection could act (*13*). In this context, a non-synonymous substitution at the *SLC39A4* gene, which encodes the most important intestinal zinc uptake transporter (ZIP4), has been shown to produce differential cellular zinc uptake and presents extreme population differentiation because of a local positive selection event in Sub-Saharan Africa (*14*, *15*).

The *SLC30A9* gene has been repeatedly reported as a top candidate region for positive selection in several genome-wide scans of selection, mostly in East Asian populations (*14*, *16–20*). This gene encodes the ZnT9 protein, a recently characterized ZT in the mitochondria (*21*, *22*). Moreover, the patterns of genetic variation and population differentiation at *SLC30A9* have also been investigated in candidate-based selection studies analyzing human adaptation in relation to zinc homeostasis (*13*, *23*, *24*). In most of these previous studies, the adaptive signals in *SLC30A9* have been attributed to a non-synonymous single nucleotide polymorphism (SNP)

(rs1047626; c.148A>G) resulting in the substitution of a methionine by a valine in the N-terminus of the ZnT9 transporter (Met50Val) (*13*, *17*, *23*, *24*). In agreement with the strong signatures of recent positive selection detected in East Asia, this non-synonymous SNP presents extremely high levels of population differentiation, where the ancestral A-allele (encoding Met) is at high frequency in African populations, whereas the derived G-allele (encoding Val) is nearly fixed in East Asian populations and at intermediate frequencies in European, South Asian, and American populations. Moreover, contrasting extended haplotypes and selection signals along the *SLC30A9* region have also been reported between Africans and East Asians (*13*). Furthermore, the derived G-allele has been shown to correlate with the distribution of human zinc deficiency worldwide (*13*) and to be in moderate linkage disequilibrium with three variants in the 3' flanking region of the *SLC30A9* gene, which are QTLs influencing zinc content in the liver (*23*). However, to date, no experimental validation has been performed to demonstrate the functional relevance of this putative adaptive variant regarding zinc transport.

Here, we first compiled evidence for a selective sweep in the *SLC30A9* gene region, inferred the past allele trajectories and selection coefficients for two putative adaptive SNP variants characterizing the two major *SLC30A9* haplotypes in humans, traced back their genetic origins and then investigated the phenotypical relevance of the Met50Val substitution (rs1047626) in ZnT9. Accordingly, we overexpressed ZnT9 in HEK293 cells and explored whether the two variants of the Met50Val substitution induce differences in the expression levels and localization of ZnT9 and other ZTs, and whether they differentially affect zinc transport in the cytosol, mitochondria, and endoplasmic reticulum (ER). Our results not only show the Met50Val candidate substitution located in an unusual haplotype, which was likely introgressed from archaic humans, but also demonstrate relevant differences in mitochondrial and ER zinc homeostasis directly influencing cellular viability.

## Results

### *Signals of positive selection outside Africa*

We first explored the genomic signatures of the selective sweep previously identified in the *SLC30A9* gene region (*14*, *16–18*, *20*, *25*). Hence, we compiled evidence from different summary statistics and selection tests available at the PopHuman browser for the 26 human populations from the 1000 Genomes Project (http://pophuman.uab.cat) (*26*). To summarize and visualize the continental patterns of positive selection along the *SLC30A9* region, we extracted the $F_{ST}$, XP-EHH, and Fay and Wu's H values in three populations used as a reference for Africa (Yoruba: YRI), Europe (Residents of Utah with North and Western European ancestry: CEU), and Asia (Han Chinese: CHB) (Figure 1A). Unusual high levels of population

differentiation were confirmed along the *SLC30A9* gene when comparing CEU and CHB with YRI. Similarly, when applying the XP-EHH statistic, we detected genome-wide departures for long haplotypes in CEU and above all in CHB (using YRI as the reference). Furthermore, a significant excess of derived alleles was detected around the *SLC30A9* gene in both CHB and CEU populations when analyzing the site frequency spectrum with Fay and Wu's H statistic. Notably, most of these signatures of positive selection for the remaining populations of the 1000 Genomes Project replicate with a similar pattern in all continental regions except Africa (data not shown).

We next investigated which candidate variants along the *SLC30A9* gene could underlie the detected signals of selection. From a total of 355 biallelic SNPs with MAF ≥ 0.02 in the *SLC30A9* gene, we initially selected those variants with high population differentiation when comparing YRI with CEU and CHB (Supplementary Material, Table S1). From the resulting 235 variants, we further considered as putatively adaptive those that were either non-synonymous, present at the UTR regions of the *SLC30A9* gene, or had a CADD Phred score ≥ 10, as such a value predicts that the variant falls within the top 10% of the most deleterious (i.e., functional) variants of the genome (*27*). A total of 18 SNPs matched our filtering criteria (Table 1). Among these, we identified a non-synonymous SNP, two synonymous variants, five variants at the 3' UTR, and ten intronic variants. According to the GTEX portal (https://www.gtexportal.org/home/; last accessed 13/04/2022), all 18 putative adaptive variants are eQTLs, with the most common allele in CHB and CEU associated with reduced *SLC30A9* expression mostly in brain (Supplementary Material, File S1). The frequencies of the derived G-allele of the non-synonymous SNP rs1047626 (coding for Val), as well as those of the remaining putative adaptive variants identified along the *SLC30A9* gene, coincide with the signatures of recent positive selection detected in CHB and CEU (Figure 1B).

We then took advantage of the previously inferred genome-wide genealogies available for the 1000 Genomes Project individuals and used Relate (*28*) to explore whether the lineages carrying the Met50Val substitution had spread at an unusually fast rate in comparison with competing lineages in the YRI, CHB and CEU populations. The marginal tree corresponding to the surrounding region of rs1047626 displayed the Val-derived variant in multiple lineages concentrated in CHB and CEU, although it was also present in some YRI haplotypes (Supplementary Material, Figure S1). In contrast, most of the lineages carrying the ancestral variant were mainly found in YRI. The subsequent analysis with CLUEs estimated positive selection acting on rs1047626 at ~56-77 kya (i.e., 2,000-2,750 generations before the present; using 28 years per generation) with selection coefficients s=0.0113 (logLR=5.68) and s=0.0017 (logLR=10.93) in CHB and CEU, respectively (Figure 1C). When analyzing other non-African populations such as FIN (European), JPT (East Asian), PJL (South Asian) and PEL (American),

we obtained similar allelic trajectories and selection coefficients (Supplementary Material, Figure S2). These results suggest that the positive selection acting on rs1047626 probably coincided with (or even predated) the expansion of modern humans out of Africa ~45-60 kya (*29*).

*Archaic introgression*

A plausible scenario that could reconcile such an early date is adaptive introgression from archaic lineages. Therefore, we explored whether the Met50Val substitution was present in the Neanderthal and Denisovan genomes available at the UCSC Genome Browser. Remarkably, all 22 Denisovan reads covering the rs1047626 position carry the derived allele, whereas the only two reads available for Neanderthals (in the Vindija 33.26 individual) carry the ancestral allele. We then further investigated the corresponding Neanderthal and Denisovan base positions for a total of 170 SNPs found in high LD ($r^2$>0.8) with rs1047626 in CHB and CEU and spanning a 98.74 kb region (Figure 1D; Supplementary Material, Table S2). For 164 of these SNPs (96%), the most frequent allele in EAS, EUR, SAS and AMR differs from the most prevalent in AFR, confirming the existence of two major contrasting Yin/Yang human haplotypes. Notably, the Neanderthal and Denisovan genomes share alleles in 96 out of 110 corresponding covered SNP positions (87%) and were found to display much higher similarity with the non-African allelic combinations. In particular, the most frequent allele found outside Africa was observed in 139 out of the 171 available SNP positions in the Denisovan genome (81%) and in 70 out of the 110 covered SNP positions in the available Neanderthal genomes (64%). Moreover, 79 out of the 139 (57%) and 44 out of the 70 (63%) alleles shared between archaic hominins and the most frequent allele outside Africa are derived in the Denisovan and Neanderthal genomes, respectively (Figure 1E; Supplementary Material, Table S2).

Given these results, we then investigated whether the *SLC30A9* region had been identified in genome scans of Neanderthal and Denisovan introgression into modern humans. No hit for *SLC30A9*, the rs10476262 position or neighboring SNPs was found within the most probable candidate genomic regions for Neanderthal introgression (*30–32*). However, two independent studies recently reported two overlapping candidate regions for Denisovan introgression in Melanesians (*33*) and Papua New Guineans (*34*), respectively, comprising the rs1047626 position (Figure 1D; Supplementary Material, Table S2 and Figure S3). Furthermore, by inspecting the allele frequencies for rs1047626 and five neighboring SNPs at *SLC30A9* available in the ALFRED database (*35*), we were able to confirm that the alleles linked to the putative selected haplotype outside Africa were indeed nearly fixed in the Oceanian populations previously inferred to present Denisovan introgression (Supplementary Material, Table S3).

*Signals of positive selection in Africa*

As signatures of positive selection had been previously reported for the most abundant haplotype of *SLC30A9* in YRI (*13*), we also searched for putative candidate variants displaying unusual past allelic trajectories in Africa. Notably, several derived allele variants characterizing the African-like haplotype of *SLC30A9* were found to show marginal genome-wide p-values for selection with Relate (Supplementary Material, Table S2). After their corresponding functional annotation, we selected one of the strongest eQTLs (i.e., rs4864457) for further analysis with CLUEs, which estimated a selection coefficient s=-0.00425 and a logLR=16.2401 for an adaptive event occurring within the last 1,000 generations (i.e. 28,000 years before present) in the YRI population (Figure 1C; Supplementary Material, Tables S4-7 and Figures S4-S6). These results confirm a pattern of contrasting directional selection acting on *SLC30A9* between African and non-African populations. Moreover, as expected, the derived allele of rs4864457 has high frequencies in all African populations from the 1000 Genome Project and associates with higher *SLC30A9* expression (as the remaining derived eQTLs predominant in Africa; Supplementary Material, Table S4 and Figure 1F).

*Molecular phenotype for Met50Val*

We then investigated whether the Met50Val substitution in ZnT9 could determine any further differential molecular phenotype to explain this case of putative adaptative archaic introgression outside Africa. We first verified the predicted protein structure of ZnT9 using the AlphaFold algorithm. We observed that the polymorphic amino acid residue affected by rs1047626 is located at the cytosolic N-terminus domain of the ZnT9 transporter (Figure 2A-B). It has been suggested that the N-terminus of the ZnT family modulates the transporter activity by facilitating either protein interactions or zinc binding (*36*, *37*). Thus, we proceeded to analyze whether the Met50Val substitution could cause any differential phenotype related to zinc homeostasis at cellular level. Accordingly, we used a heterologous expression system in HEK293 cells overexpressing each of the two ZnT9 forms resulting from the Met50Val substitution, carrying either the ancestral allele (ZnT9-50Met) or the derived allele (ZnT9-50Val). Our experiments showed no difference in protein expression between the ZnT9-50Met and ZnT9-50Val variants after their corresponding 24h transient expression (Figure 2C).

We next characterized the localization of the two ZnT9-50Met and ZnT9-50Val variants. For that, we performed immunostaining in non-permeabilizing and permeabilizing conditions. The results, shown in Figure 2D, indicate that the ZnT9 N-terminus is located intracellularly and follows a reticular pattern independently of the overexpressed variant. We further explored the subcellular distribution of the variants co-transfecting the ZnT9 constructs with the FEMP probe, a double fluorescent reporter plasmid for the ER (in CFP) and the mitochondria (in YFP). Our colocalization analysis gave similar results for the two ZnT9 variants, both showing a higher colocalization degree with the ER compartment (Supplementary Material, Figure S7).

We then used super-resolution STED microscopy to confirm the presence of ZnT9 in mitochondria as described by others (*21*, *22*) (Figure 3). ZnT9-HA was co-stained with anti-TOM20 (Figure 3A), a mitochondrial outer membrane resident protein. Both ZnT9-50Met and ZnT9-50Val variants showed co-localization with mitochondria. Remarkably, by analyzing the mean distance between mitochondria (Figure 3B) and the relative area occupied by mitochondria in the cell (Figure 3C), we observed that the overexpression of ZnT9 generated mitochondrial clustering in comparison with cells non-transfected. In order to check whether the distance between ER and mitochondria might be altered we carried out FRET analysis using the FEMP probe together with the ZnT9 variants or empty vector. Our results showed no differences in any of the tested conditions (Figure 3E). Overall, this initial characterization revealed no differences in cellular localization for either variant.

We then studied the impact of ZnT9 overexpression on cellular zinc homeostasis, comparing cells transiently transfected with either of the ZnT9 variants or an empty vector. First, the mRNA expression of the different ZIP transporters was characterized to analyze whether the overexpression of ZnT9, a transporter reported to promote cytosolic zinc efflux, is somehow compensated for by a modification in a zinc importer expression (Figure 4A). Our results showed alterations in ZIP12 and ZIP14 expression, although in the case of ZIP12 CT values were above 30 and ZIP14 displayed a reduction in cells overexpressing either of the two ZnT9 variants. We then used flow cytometry with Zinquin to measure the cytosolic zinc content in basal conditions or with excess zinc for 30 min and observed no differences in cytosolic zinc handling between vectors in the two tested conditions (Figure 4B).

Given the presence of the ZnT9 transporter in ER membranes, we measured the endoplasmic zinc content using ER-ZapCY1 probe. No major alterations were observed in cells transfected with ZnT9-50Val, ZnT9-50Met, or an empty vector in basal conditions. However, upon incubation with 100 µM external zinc medium, only the cells transfected with ZnT9-50Met or an empty vector had an increased ER zinc content, indicating that the overexpression of ZnT9-50Val was modifying the ER zinc homeostasis (Figure 4C). When analyzing the RNA expression of the known ER zinc importers ZnT5, ZnT6 and ZnT7, we found that the overexpression of ZnT9-50Val causes a downregulation of ZnT5 and ZnT6 expression (Figure 4D). Considering that ZIP7 is the major zinc exporter in the ER, we further explored its activity in conditions of ZnT9 overexpression. After 24h of transient expression, the results showed no difference in ZIP7 protein expression between the ZnT9 variants (Supplementary Material, Figure S8A). We also measured the ER zinc content in the presence of a ZIP7 blocker, finding a strong increase in the fluorescence of the ER zinc reporter. However, differences between basal and 100 µM external zinc conditions were no longer observed, nor between ZnT9 variants and

the empty vector (Figure 4E), indicating that in the absence of ZIP7 activity the ER suffers a zinc overload.

As ZnT9 has been shown to regulate mitochondrial zinc homeostasis (*21*, *22*), we also interrogated the functional relevance of the Met50Val substitution by measuring the zinc content in the intermembrane space and the mitochondrial matrix, using SMAC-mCherry-GZnP2 and mito-Cherry-GZnP2 probes, respectively. In the intermembrane space, overexpression of ZnT9-50Val, resulted in a slightly higher zinc content than cells overexpressing ZnT9-50Met, or an empty vector. However, zinc increased equally in all conditions upon incubation with 100 µM zinc (Figure 4F). In the mitochondrial matrix, ZnT9-50Val-transfected cells had a higher zinc content in basal conditions as well but that was not further affected by incubating with 100 µM zinc, contrary to cells overexpressing ZnT9-50Met, or an empty vector (Figure 4G). Given that mitochondrial zinc content is reported to depend on ER zinc transport (*21*, *22*), similar experiments were carried out, but this time blocking the ER zinc exporter ZIP7 for 30 min to accumulate zinc in this organelle. The result was an increase of zinc levels in the mitochondrial matrix of control cells but not in ZnT9 overexpressing cells (Supplementary Material, Figure S8B). To gain further insight into the ZnT9 transport activity in the mitochondria, ZnT9 was silenced with siRNA and the zinc content of the mitochondrial matrix was measured. As the data showed that incubation with 100 uM zinc increases zinc levels despite silencing ZnT9, we discarded the possibility that ZnT9 is a major zinc importer in the mitochondria (Supplementary Material, Figure S9A). Our expression data confirmed the silencing strategy and showed no alterations in the expression of ZnT5, the zinc importer in the ER, when ZnT9 was silenced (Supplementary Material, Figure S9B). Finally, we investigated the impact of ZnT9 variant overexpression on cell viability. MTT experiments were carried out in cells incubated for 24h with 0, basal and 100 uM zinc content. Higher viability was found in ZnT9-50Val-overexpressing cells both in basal and zinc excess conditions compared with the control (Figure 4H). The absence of difference in the 0 zinc media supports the idea that the impact on viability is due to a zinc-dependent process.

*Exploring an adaptive phenotype for Met50Val*

As three SNPs in the 3' flanking region of the *SLC30A9* gene (rs2880666, rs6447133, rs7659700) have been previously identified as QTLs influencing zinc content in the liver (*23*) and they are found in moderate linkage disequilibrium ($0.66 < r^2 < 0.76$) with rs1047626 (Supplementary Material, Table S8), we also examined whether rs1047626 could be associated with such a systemic phenotype. No significant differences in liver zinc content were detected between individuals carrying A- or G-alleles (p-value=0.107), nor between the AA, AG, and GG genotypes at rs1047626 (p-value=0.322). However, in agreement with the known effects of

the surrounding nutriQTLs with which the alleles at rs1047626 associate, the homozygous individuals for the G-allele showed a tendency towards higher zinc concentrations in the liver than those homozygous for the A-allele, whereas the heterozygotes AG were associated with an intermediate zinc content (Supplementary Material, Table S9, Figure S10). Additionally, we searched for GWAS annotations linked to any of the 170 SNPs in high linkage disequilibrium ($r^2 > 0.8$) with rs1047626. We found reported GWAS hits for helping behavior (rs1507086, rs2660319, rs11051), total PHF-tau SNP interaction (rs4861153), and one SNP (rs34215985) associated with multiple psychiatric phenotypes, such as anorexia nervosa, hyperactivity disorder, autism spectrum disorder, bipolar disorder, major depression, obsessive compulsive disorder and schizophrenia. A phenome-wide association study (PheWAS) for rs1047626 retrieved seven entries with a corrected p-value $\leq 1.5 \times 10^{-5}$ (0.05/3,302 unique traits), including traits within the psychiatric (i.e., neuroticism and major depressive disorder, being the derived G-allele of the rs1047626 polymorphism the allele that increases the risk of both phenotypes), metabolic (i.e., impedance, with the G-allele associated with lower impedance measures), activities (i.e., fish oil, and glucosamine uptake, with the G-allele increasing the phenotype value) and skeletal (i.e., height, with the G-allele decreasing the phenotype value) domains, respectively (Supplementary Material, Table S10).

## Discussion

The motivation for this study was the previous detection of strong signatures of positive selection in the *SLC30A9* region (*13*, *14*, *16*, *17*, *20*, *25*). In this context, we first re-examined the genetic evidence for a hard-selective sweep using the $F_{ST}$, XP-EHH, and Fay and Wu's H selection statistics and found several functional variants on *SLC30A9* that could explain the strong adaptive signals detected. In accordance with previous studies (*13*), we confirmed contrasting signals of positive selection between two major haplotypes in Africa and East Asia, the latter also being present at intermediate-high frequencies in South Asia, Europe, and America. The major African haplotype carries alleles at several eQTLs associated with higher *SLC30A9* expression in different brain areas. In contrast, the most prevalent allelic combinations outside Africa are associated with lower gene expression and are linked to the derived allele of the rs1047626 polymorphism, which causes a Met to Val substitution at codon position 50. Although no experimental characterization of its corresponding molecular phenotype has been reported to date, previous studies have attributed the strong signals of adaptation found in East Asians to this non-synonymous variant (*13*, *17*, *23*). In the present work, we describe the presence of the derived Val allele in the Denisovan genome and an unusually high sharing of derived alleles between the major haplotype outside Africa and

archaic humans (both Neanderthals and Denisovans). Such pattern is compatible with two independent studies reporting a Denisovan adaptive introgressed region in modern Melanesians (*33*) and Papua New Guineans (*34*) overlapping with the *SLC30A9* gene and comprising the rs1047626 polymorphism.

The protein structure of ZnT9 has generated some debate, with some studies assuming it contains only 5 transmembrane domains (TMD) and a periplasmic N-terminus, based on older prediction algorithms (*13*). Such a 5 TMD structure would differ from the rest of the ZnT family members. However, a recent approach for protein structure prediction, AlphaFold (*38*), shows a total of 6 TMD and a cytosolic N-terminus for ZnT9, a structure similar to that of other members of the ZnT family. Furthermore, the first 3D structure of a human ZnT transporter, ZnT8, provided new insights into the specificities of the transporter family (*37*). For example, it was proposed that the N-terminus domain is involved in facilitating zinc transport (ZnT8) or in the dimerization or formation of protein interactions (ZnT5). Therefore, the location of the Met50Val substitution in the N-terminus may indicate a putative effect of this non-synonymous SNP on zinc homeostasis through a possible accessory role of the N-terminus domain of ZnT9 in facilitating zinc transport or protein interactions.

When analyzing the consequences of the Met50Val substitution at the molecular level, the expression studies revealed a similar partial localization of both ZnT9 variants in the ER and mitochondria. Moreover, we observed mitochondrial clustering near the ER when ZnT9 was overexpressed. The presence of the transporter in both cellular compartments has been previously described (*39*), and the ionic fluxes between the two organelles are highly interconnected. In this context, it has been recently described that the ZnT9KO phenotype can be rescued by targeting transporters in the ER and mitochondria (*22*). The ER plays a major role in protein folding, maturation, quality control, and trafficking. Many of these processes require zinc to function correctly, and its deficit or excess often leads to protein malformations that induce ER stress. The most well-known ZTs implicated in ER zinc homeostasis are the ZnT5-ZnT6 heterodimer and ZnT7 homodimer, which are involved in zinc importation (*40*, *41*), and ZIP7, which is the main zinc-releasing transporter in the ER (*42*). Considering the effect on ER zinc homeostasis of the overexpression of either ZnT9 isoform, we propose that the 50Val variant avoids ER zinc accumulation due to the reduced ZnT5-ZnT6 heterodimer expression. Additionally, we observed that ZIP7 inhibition generates an excess of zinc in the ER, supporting the idea that the zinc exporting activity of ZIP7 is key for maintaining endoplasmic zinc homeostasis. Therefore, it is likely that the observed absence of differences in ER zinc content in basal conditions is due to the master role of ZIP7 in fine-tuning ER zinc content.

It has been proposed that ZnT9 in the mitochondria together with ZnT5 in the ER determine the zinc content in the mitochondrial matrix (*22*). ZnT9 has been identified as a zinc exporter from the mitochondria based on the zinc accumulation observed in the mitochondria in ZnT9KO models (*21*, *22*, *39*). We only detected a mild increase in zinc in ZnT9-silenced cells, which was not statistically significant. Probably, the zinc accumulation observed in KO models is the result of a complete and chronic effect. Nevertheless, this transport model implies that ZnT9 works in the opposite direction from the rest of the ZnT transport family. Our results showed that ZnT9 50Val expression increases the zinc content of the mitochondrial matrix but avoids zinc overload. The intermembrane space, however, showed no differences at high zinc concentrations between the tested conditions. Zinc homeostasis in this space has been previously reported to follow cytosolic zinc concentrations (*43*). On the other hand, it is likely that the repression of ZnT5 expression observed in ZnT9 50Val cells might be a negative feedback to avoid a further zinc increase in the mitochondrial matrix. Having ruled out that ZnT9 is a zinc importer, we speculate that it might influence a wider machinery of proteins involved in mitochondrial zinc homeostasis. Altogether, our data indicate that more studies are required to fully understand zinc dynamics in this compartment. Importantly, we show that the ZnT9 50Val variant increases cell viability in a zinc-dependent manner. ZnT9 has been previously reported to affect mitochondrial function (*21*, *22*) and here we show that it also affects zinc homeostasis in the ER. Both organelles are interconnected and essential for cell fate and metabolism (*44*).

In a recent study, a mutation in the fourth TMD in *SLC30A9* was found in all the members of a family affected by a novel cerebro-renal syndrome with important early neurological deterioration (*45*). It was demonstrated that this mutation generated acute dysregulation of zinc homeostasis, leading to the serious phenotypic consequences observed in the patients. Given that the Met50Val substitution is located in what is expected to be an auxiliary region for the activity of the transporter, we hypothesize that the effects of rs1047626 on zinc homeostasis are milder, but somehow became adaptive in the past. In fact, when analyzing whether the genotype for rs1047626 influenced zinc content in the liver as a proxy for systemic zinc homeostasis, we only detected a tendency towards increased zinc in the liver when the derived G-allele (50Val) was present. Even if larger sample sizes might produce results with significant differences, any putative effect of rs1047626 on liver zinc content would be lower than that of the QTLs previously identified in the 3´region of the *SLC30A9* gene. Although *SLC30A9* is moderately expressed in most tissues, its expression is higher in the fetal brain, cerebellum, skeletal muscle, pituitary, thyroid, and kidneys (*45*). Hence, greater effects of the Met50Val substitution on other tissues or organs cannot be ruled out, for instance, related to adjustments in renal excretion, brain function or even skeletal muscle metabolism. Indeed, the major haplotype

outside Africa was found to be significantly associated with greater susceptibility to major depression and other related psychiatric disorders (*46*, *47*) as well as with higher values for self-reported helping behavior (*48*). Furthermore, our PheWAS analysis reveals that the derived G-allele of rs1047626 contributes not only to a greater risk for both major depressive disorder and neuroticism but also lower impedance (i.e., a higher lean body mass), among others. Neuroticism might have been beneficial in ancestral environments, for instance high neuroticism may have been necessary for avoidance of acute dangers (*49*).

Despite all the data we have compiled, it is not obvious how the differential molecular phenotype for the Met50Val substitution can be translated into an adaptive phenotype at the organism level. Remarkably, zinc accumulates in glutamate synaptic vesicles and modulates excitability (*50*). Glutamate is the major excitatory neurotransmitter in the central nervous system and it is essential for cognition and emotion (*51*). Also, glutamate excitotoxicity has been shown to be partially mediated by zinc overload in the postsynaptic neuron (*52*). Thus, a putative adaptive function of Met50Val substitution to reduce zinc-mediated excitotoxicity is an attractive hypothesis that deserves further studies. We could speculate that the derived G-allele, which we have shown provides better protection to the mitochondria, could help to overcome zinc overload derived from excitotoxicity, ischemia or exacerbated ROS production (*52*). Interestingly, dysfunctional glutamatergic signaling is associated with neuropsychiatric conditions such as schizophrenia, major depression and anxiety among others (*51*, *53*, *54*). Moreover, considering the involvement of the mitochondria in the pathogenesis of several neuropsychiatric disorders (*55*–*57*), the differential molecular phenotypes of the Met50Val substitution reported here may help to provide mechanistic links to these associated traits. Alternatively, given the essential role of mitochondria in both skeletal muscle and brown adipose tissue thermogenesis, we could also speculate that the derived G-allele could have been positively selected to facilitate adaptation to cold. This is a plausible scenario for a case of archaic adaptive introgression, as Denisovans and Neanderthals were probably already well adapted to the local environmental conditions modern humans encountered when expanding across Eurasia. In conjunction with the previous scenario, emotional learning could also have been advantageous in promoting social interaction and cooperation among the modern human groups expanding outside Africa.

In conclusion, we report that the signatures of positive selection recognized in the *SLC30A9* gene region outside Africa are associated with differential zinc homeostasis in the mitochondria and endoplasmic reticulum mediated by the Met50Val substitution. Although several promising traits have been associated with rs1047626, additional work is required to understand how such a molecular phenotype is refined into an adaptive phenotype. Moreover, it cannot be ruled out

the possible adaptive role of regulatory variants, influencing both *SLC30A9* expression and liver zinc content (and thus systemic homeostasis of zinc), also contributing to the adaptive phenotype we proposed for the Met50Val substitution. Finally, further work is necessary to ascertain the exact timing and particular admixture events experienced with archaic humans, which could explain the patterns of variation along the *SLC30A9* gene and the contrasting signatures of positive selection detected in modern human populations in and outside Africa.

## Methods

### *Signals of positive selection in the SLC30A9 region*

The PopHuman genome browser (http://pophuman.uab.cat) (*26*) was consulted to search for signatures of recent positive natural selection along the *SLC30A9* region. This browser contains a broad range of genomic metrics and neutrality tests for all 26 human populations of the 1000 Genomes Project (The 1000 Genomes Project Consortium 2015). Window-based computed values for $F_{ST}$, XP-EHH, and Fay and Wu's H statistics were extracted from three geographically differentiated populations from Africa, Europe, and Asia: the Yoruba from Ibadan (YRI), Utah residents with Northern and Western European ancestry (CEU), and Han Chinese from Bejing (CHB). Furthermore, gene annotations surrounding the *SLC30A9* region were obtained from the Ensembl genome browser (http://grch37.ensembl.org/). The collected information was then represented using the Gviz package (Hahne and Ivanek 2016). For each selection statistic and population, deviations from neutrality were considered as those greater than two standard deviations from the genomic mean.

### *Analysis of putative adaptive variants in SLC30A9*

All Single Nucleotide Polymorphisms (SNPs) for the longest *SLC30A9* gene transcript (ENST00000264451) were extracted from the Ensembl Genome Browser (GRCh37 assembly). Only biallelic variants with a MAF $\geq$ 0.02 were kept for further analysis and subsequently annotated using ANNOVAR (Wang et al. 2010) to obtain their corresponding genomic location, SNP type classification (i.e. coding, non-coding, synonymous, non-synonymous), and allele frequency information. Next, all compiled variants were explored for associations in the GWAS Catalog (v1.0) and eQTLS in the GTEx Portal Dataset (V7) and they were further annotated with different *in silico* function predictors such as the score of Combined Annotation-Dependent Depletion (CADD score) (*27*), the Eigen score (*58*), and the FitCons score (*59*). Pairwise linkage disequilibrium ($r^2$) data in CEU between each candidate variant and rs2880666, rs6447133, rs7659700 was also extracted from Ensembl.

*Selection on rs1047626 and rs4861157*

We used Relate (28; https://myersgroup.github.io/relate) to test whether rs1047626 and rs4861157 were detected as fast spreading variants along multiple lineages when compared to competing non-carriers. For that, we first obtained the Relate-estimated coalescence rates, haplotypes and genealogies available for the 1000 Genomes Project (kindly provided by Leo Speidel), removed all sample haplotypes not belonging to the CEU, CHB or YRI populations (with RelateFileFormats --mode RemoveSamples), annotated SNPs as recommended in order to later extract trees (with RelateFileFormats --mode GenerateSNPAnnotations) and the inferred genealogies for rs1047626 and rs4861157 for the populations CHB, CEU and YRI (with RelateExtract --mode SubTreesForSubpopulation --years_per_gen 28), which were then visualized (with RelateTreeViewMutation -m 1.25E-8). Subsequently, we ran CLUES (Stern et al., 2019) to estimate the corresponding selection coefficients and allelic trajectories in either CEU and CHB or YRI using the SampleBranchLengths output from Relate as obtained with the Inference.py with N 30.000.

*Introgression*

SNPs at high linkage disequilibrium ($r^2$>0.8) with rs1047626 in CEU and CHB were extracted from Ensembl, whereas their corresponding allelic states in the Neanderthal and Denisovan genomes were queried at the sequencing reads available at the UCSC Human Genome Browser GRCh37/hg19 (https://genome.ucsc.edu/; last accessed 29/04/2022). Available introgression regions inferred with ARGweaver around the *SLC30A9* region were searched and visualized with the UCSC Genome browser track indicated at Hubisz et al., 2020(last accessed 12/05/2022). Allele frequencies at rs10476262 and 5 neighbouring SNPs at *SLC30A9* in diverse human populations, including three populations from Oceania, were extracted from the ALFRED database (https://alfred.med.yale.edu/alfred/index.asp; 35).

*GWAS analysis*

We used the GWAS catalog (https://www.ebi.ac.uk/gwas/; 59) and the PheWAS option in the GWAS atlas (https://atlas.ctglab.nl/; 60) to look for trait associations with rs1047626 and SNPs in LD $r^2$ >0.8. In the PheWAS analysis, a total of 3,302 unique traits as available at the GWAS Atlas database (last accession on 16/05/2022) were considered for Bonferroni multiple test correction (FDR=1.5 x $10^{-5}$).

*Generation of polymorphic sites*

The plasmid containing the human *SLC30A9* gene codifying for the ZnT9 transporter with an N-HA tag was obtained from Sino Biological Inc. (Catalog nr. HG22621-NY). The Met50Val polymorphism was generated via site-directed mutagenesis following standard conditions (QuikChange Lightning; Agilent) with the following primers: forward primer (5'-GACATTTGGAAGCTTTTCAAACGTGGTTCCCTGTAGTCA-3') and reverse primer (5'-TGACTACAGGGAACCACGTTTGAAAAGCTTCCAAATGTC-3'). Before being used for cell transfection, both ZnT9-50Met and ZnT9-50Val isoforms were confirmed by sequencing. The LightRun sequencing service of Eurofins Genomics was used following the standard conditions for purified plasmid DNA samples with the following primers: forward primer 5'-GGCACAGAACTCAAAGCT-3' and reverse primer 5'-TCTTCATGGGGACTTCGT-3'.

*Genotyping of DNA liver samples*

DNA samples and information regarding zinc concentration in the liver were obtained from the project of Engelken and colleagues (2016), which determined micronutrient concentrations in liver samples from healthy individuals of western European origin, originally gathered by the UKHTB (for details, see Engelken et al. 2016). DNA concentrations for 143 available samples from the original study were quantified using a NanoDrop One spectrophotometer (Thermo Fisher Scientific, Waltham, MA, USA). A genomic region of 226 bp comprising the rs1047626 position was amplified, purified, and sequenced using the LightRun sequencing service (Eurofins Genomics) following standard conditions for purified PCR products. The primers used for amplification were: forward primer 5'-GAAGCAGTGAAACACCTCTGG-3', reverse primer 5'-TGTTTGTGATCCCTGTCCTTC-3'. The primer used for sequencing was 5'-TGCAGCTAGGACTTGGTTTG-3'. Genotypes for rs1047626 and the corresponding corrected zinc content per sample determined by Engelken et al. (2016) can be consulted in Supplementary Material, Table S9.

*Cell culture and transfection procedure*

HEK293 cells were cultured in DMEM supplemented with 10% FBS, 1% L-glutamine, and 1% penicillin and streptomycin (Basal medium) at 37 °C in a humidified 5% $CO_2$ atmosphere. $ZnSO_4$ was added as needed to the final medium to generate specific $Zn^{2+}$ concentration conditions.

Cells were transiently transfected with ZnT9-50Met, ZnT9-50Val, pEGFP, or empty pCDNA3 vectors depending on the experiment. Polyethyleneimine (PEI) was used as the transfection reagent using 3 μg DNA for a 6-well plate or 1 μg DNA for a 24-well plate. In RNA interference experiments we used siRNA control (1027310, Qiagen) and siRNA ZnT9 (114789, Eupheria Biotech), and the transfection reagent was Lipofectamine 3000. Cells were incubated with the transfection solution for 3 hours, then washed and replaced with normal media. The experiments were performed 24h after transfection.

To characterize the genotype of cells used for all the experiments, the DNA of HEK293 cells was extracted and purified following the NucleoSpin Tissue protocol (Macherey-Nagel, Düren, Germany). The genotype of the rs1047626 position was verified to be heterozygote (AG) in HEK293 cells with the same sequencing procedure previously described for the liver DNA samples.

*Western Blotting*

Transfected cells were grown in 6-well plates and incubated for 24 hours. Cell lysis to detect ZnT9 protein was performed with 30 μL of lysis buffer containing 50 mM Tris-HCl at pH 7.4, 150 mM NaCl, 0.5% Nonidet P-40, and EDTA-free protease inhibition cocktail (Roche). Cell lysates were vortexed for 30 min at 4 °C and centrifuged at 10,000× *g* to remove aggregates and boiled for 5 min at 95 °C to lastly be placed on ice for 1 min. After electrophoresis in 12.5% polyacrylamide gel, proteins were transferred to nitrocellulose membranes using the iBlot system (Invitrogen, Waltham, MA, USA). Membranes were blocked with either 5% milk in TBS-Tween 0.1%, for GAPDH, or 5% BSA for HA-ZnT9, for 1 hour at room temperature. Primary antibodies were diluted in the corresponding blocking solution anti-HA for ZnT9 (H3663, Sigma-Merck), and anti-GAPDH (ab8245, Abcam). HRP secondary antibodies (1:1000; GE Healthcare) were used depending on the primary antibody. The ChemiDoc XRS+ system (Bio-Rad, Hercules, CA, USA) was used to obtain high-quality images. Quantity One Software (Bio-Rad) was used to analyze the results.

*Immunostaining*

For immunodetection of the two isoforms of ZnT9, for both cell surface and total cell expression, immunostaining was performed 24 hours after transfection with ZnT9-50Met or ZnT9-50Val plasmids in 24-well plates with coverslips coated with collagen. For cell surface expression, cells were incubated with anti HA (1:1000) in DMEM for 1h at 37°C. All samples were fixed with 4% paraformaldehyde (PFA) and only for total cell expression experiments were cells permeabilized with 0.1% Triton x-100 in PBS for 10 minutes. For all experiments,

samples were blocked overnight with 1% BSA and 2% FBS in PBS. For total cell expression experiments, samples were incubated for 1h with an anti-HA antibody (1:1000 in blocking solution). For all experiments, cells were incubated with the secondary antibody (1:2000 in blocking solution), a goat anti-mouse Alexa Fluor 488 (Molecular Probes). Images were acquired using an inverted Leica SP8 Confocal Microscope with a 63× Oil objective and analyzed using ImageJ software.

In the colocalization analysis, to determine the subcellular distribution of the variants, immunostaining was performed 24 hours after transfection in 24-well plates with coverslips. Cells were co-transfected with ZnT9-50Met or ZnT9-50Val plasmids and a modified FRET-based ER-mitochondria proximity probe named FEMP (*62*). The immunostaining procedure was the same as the one described above, except for the secondary antibody, which in this case was a goat anti-mouse Alexa Fluor 555 (Molecular Probes). The analysis of colocalization of ZnT9 with either the ER or mitochondria was performed with both Pearson's correlation coefficient and Mander's overlap coefficient using ImageJ software.

For STED imaging, cells were grown and seeded on 1.5H-thickness cover glasses. Primary antibodies were diluted in 2% BSA blocking buffer reagent. We used the rabbit anti-human TOM20 and the rabbit anti-human Calreticulin antibodies (1:1000) and secondary antibodies Abberior STAR RED or ORANGE (1:350). STED images were taken with a commercial Leica TCS SP8 STED 3× microscope equipped with a pulsed supercontinuum white light laser excitation source, using a 100× 1.4 NA oil HC PL APO CS2 objective. Post-analysis was performed on ImageJ. In order to measure the area occupied by the mitochondria, with the Freehanded selection tool we measured the cell region on the HA channel, subtracted the nucleus area and selected the area occupied by these organelles. The distribution of the mitochondria was quantified tracing a segmented line that connected all single mitochondria in one cell and then compare the length of these lines against the length in control cells.

*Real-Time RT PCR*

Cells transfected with either ZnT9-50Met, ZnT9-50Val, or empty pCDNA3 vectors were grown in 6-well plates and incubated for 24 hours. Total RNA was extracted from cells using Macherey-Nagel total RNA extraction kit. RNA was measured using a NanoDrop 1000 spectrophotometer (Thermo Fisher). cDNA was generated using a SuperScript Reverse Transcriptase system (Invitrogen). Quantitative PCR was performed using SYBR Green (Applied Biosystems) in the QuantStudio 12K system (Applied Biosystems). Primers are listed in Supplementary Material, Table S11.

*Zinc Measurements*

For the detection of zinc at the cytosolic level, cells were co-transfected with ZnT9-50Met or ZnT9-50Val vectors and pEGFP in 24-well plates. 24 hours after transfection, cells were incubated with 25 µM of Zinquin (Sigma-Aldrich, Darmstadt, Germany) for 30 min at 37 °C (5% $CO_2$) in isotonic solution (ISO) containing 140 mM NaCl, 2.5 mM KCl, 1.2 mM $CaCl_2$, 0.5 mM $MgCl_2$, 5 mM glucose, and 10 mM Hepes (300 milliosmoles/liter, pH 7.4), and different concentrations of $Zn^{2+}$. Cells were then dissociated with Trypsin 0.05% in 0.53 mM EDTA and washed with PBS. Fluorescence was quantified using an LSRII flow cytometer. Further analysis was performed using Flowing software to quantify Zinquin fluorescence of live transfected cells (Perttu Terho, Turun yliopisto, Turku, Finland).

To determine ER zinc levels, *in vivo* confocal imaging was used in cells co-transfected with the FRET-based ER-ZapCY1 probe (Addgene, Catalog nr. 36321)(*63*) and ZnT9-50Met, ZnT9-50Val, or empty pCDNA3 vectors in 6-well plates with 22 mm coverslips. 24 hours after transfection, cells were incubated with basal medium or supplemented with 100 µM $ZnSO_4$ for 3 hours. Then, samples were placed under the microscope in ISO for imaging with an SP8 Leica microscope (Wetzlar, Germany). When blocking ZIP7 activity, 1 µM of the ZIP7 inhibitor NVS-ZP7-4; HY-114395, MedChemExpress (Quimigen) or 1 µM of DMSO used as a control were added at 1:1000 in the treatment 3 hours before imaging. The measured zinc content is dependent on the FRET signal, which is expressed as the mean of YFP/CFP ratios from each condition normalized across experiments to an empty vector in basal zinc conditions. Images were analyzed using ImageJ software.

Mitochondria zinc concentration was measured *in vivo* using a plate reader (VICTOR Nivo, Perkin Elmer). Cells were co-transfected with Mito-cCherry-Gn2Zn or SMAC-Gn2Zn probes (*43*)and ZnT9-50Met, ZnT9-50Val, or empty pCDNA3 vectors in 24-well plates. 24 hours after transfection, cells were incubated for 40 min with basal medium or supplemented with 100 µM $ZnSO_4$. Then the media was changed to ISO solution and samples were placed in the plate reader for measuring. When blocking the ZIP7 activity, 1µM of the ZIP7 inhibitor NVS-ZP7-4 or DMSO was used as a control. Zinc content is expressed as the mean of GFP/Cherry ratios from each condition normalized to an empty vector in basal zinc conditions.

*MTT assays*

Cells were transfected with ZnT9-50Met, ZnT9-50Val, or empty pCDNA3 vectors in 24-well plates and incubated for 24h with normal medium, supplemented with 100 µM ZnSO4 or $Zn^{2+}$-

free growth medium generated with Chelex 100 resin. Then, 3-(4,5-dimethylthiazol-2-yl)-2,5-diphenyltetrazolium bromide (MTT) reagent was added (0.5 mg/mL) for 2 h at 37 °C. After that, the supernatant was removed, and cells were resuspended in 400 µl of DMSO. The absorbance was read at 570 nm.

**References**


1. J. S. Rees, S. Castellano, A. M. Andrés, The Genomics of Human Local Adaptation. *Trends in Genetics* (2020), doi:10.1016/j.tig.2020.03.006.
2. J. J. Vitti, S. R. Grossman, P. C. Sabeti, Detecting Natural Selection in Genomic Data. *Annual Review of Genetics*. **47**, 97–120 (2013).
3. J. M. Akey, Constructing genomic maps of positive selection in humans: Where do we go from here? *Genome Research*. **19**, 711–722 (2009).
4. S. Fan, M. E. B. Hansen, Y. Lo, S. A. Tishkoff, Going global by adapting local: A review of recent human adaptation. *Science (1979)*. **354**, 54–59 (2016).
5. J. Lachance, S. A. Tishkoff, Population Genomics of Human Adaptation. *Annual Review of Ecology, Evolution, and Systematics*. **44**, 123–43 (2013).
6. International Zinc Nutrition Consultative Group (IZiNCG), *Assessment of the Risk of Zinc Deficiency in Populations and Options for Its Control* (2004), vol. 25.
7. T. Kambe, T. Tsuji, A. Hashimoto, N. Itsumura, The Physiological, Biochemical, and Molecular Roles of Zinc Transporters in Zinc Homeostasis and Metabolism. *Physiological Reviews*. **95**, 749–784 (2015).
8. B. L. Vallee, K. H. Falchuk, The Biochemical Basis of Zinc Physiology. *Physiological Reviews*. **73**, 79–118 (1993).
9. T. Hara, T.-A. Takeda, T. Takagishi, K. Fukue, T. Kambe, T. Fukada, Physiological roles of zinc transporters: molecular and genetic importance in zinc homeostasis. *J Physiol Sci*. **67**, 283–301 (2017).
10. T. Fukada, T. Kambe, Molecular and genetic features of zinc transporters in physiology and pathogenesis. *Metallomics*. **3**, 662–674 (2011).
11. L. Huang, S. Tepaamorndech, The SLC30 family of zinc transporters-A review of current understanding of their biological and pathophysiological roles. *Molecular Aspects of Medicine*. **34**, 548–560 (2013).
12. J. Jeong, D. J. Eide, The SLC39 family of zinc transporters. *Molecular Aspects of Medicine*. **34**, 612–619 (2013).
13. C. Zhang, J. Li, L. Tian, D. Lu, K. Yuan, Y. Yuan, S. Xu, Differential natural selection of human zinc transporter genes between african and non-African populations. *Scientific Reports*. **5**, 9658 (2015).
14. L. B. Barreiro, G. Laval, H. Ne Quach, E. Patin, L. Quintana-Murci, Natural selection has driven population differentiation in modern humans. *Nature Genetics*. **40**, 340–345 (2008).
15. J. Engelken, E. Carnero-Montoro, M. Pybus, G. K. Andrews, C. Lalueza-Fox, D. Comas, I. Sekler, M. de la Rasilla, A. Rosas, M. Stoneking, M. A. Valverde, R. Vicente, E. Bosch, Extreme population differences in the human zinc transporter ZIP4 (SLC39A4) are explained by positive selection in Sub-Saharan Africa. *PLoS Genet*. **10**, e1004128 (2014).

16. C. S. Carlson, D. J. Thomas, M. A. Eberle, J. E. Swanson, R. J. Livingston, M. J. Rieder, D. A. Nickerson, Genomic regions exhibiting positive selection identified from dense genotype data. *Genome Research*. **15**, 1553–1565 (2005).
17. S. R. Grossman, K. G. Andersen, I. Shlyakhter, S. Tabrizi, S. Winnicki, A. Yen, D. J. Park, D. Griesemer, E. K. Karlsson, S. H. Wong, M. Cabili, R. A. Adegbola, R. N. K. Bamezai, A. V. S. Hill, F. O. Vannberg, J. L. Rinn, E. S. Lander, S. F. Schaffner, P. C. Sabeti, Identifying Recent Adaptations in Large-Scale Genomic Data. *Cell*. **152**, 703–713 (2013).
18. J. K. Pickrell, G. Coop, J. Novembre, S. Kudaravalli, J. Z. Li, D. Absher, B. S. Srinivasan, G. S. Barsh, R. M. Myers, M. W. Feldman, J. K. Pritchard, Signals of recent positive selection in a worldwide sample of human populations. *Genome Research*, 826–837 (2009).
19. P. C. Sabeti, P. Varilly, B. Fry, J. Lohmueller, E. Hostetter, C. Cotsapas, X. Xie, E. H. Byrne, S. A. McCarroll, R. Gaudet, S. F. Schaffner, E. S. Lander, T. I. H. Consortium, Genome-wide detection and characterization of positive selection in human populations. *Nature*. **449**, 913–8 (2007).
20. S. H. Williamson, M. J. Hubisz, A. G. Clark, B. A. Payseur, C. D. Bustamante, R. Nielsen, Localizing Recent Adaptive Evolution in the Human Genome. *PLoS Genetics*. **3**, e90 (2007).
21. H. Deng, X. Qiao, T. Xie, W. Fu, H. Li, Y. Zhao, M. Guo, Y. Feng, L. Chen, Y. Zhao, L. Miao, C. Chen, K. Shen, X. Wang, SLC-30A9 is required for Zn2+ homeostasis, Zn2+ mobilization, and mitochondrial health. *Proc Natl Acad Sci U S A*. **118** (2021), doi:10.1073/pnas.2023909118.
22. T. Ma, L. Zhao, J. Zhang, R. Tang, X. Wang, N. Liu, Q. Zhang, F. Wang, M. Li, Q. Shan, Y. Yang, Q. Yin, L. Yang, Q. Gan, C. Yang, A pair of transporters controls mitochondrial Zn 2+ levels to maintain mitochondrial homeostasis. *Protein Cell* (2021), doi:10.1007/S13238-021-00881-4.
23. J. Engelken, G. Espadas, F. M. Mancuso, N. Bonet, A. L. Scherr, V. Jimenez-Alvarez, M. Codina-Sola, D. Medina-Stacey, N. Spataro, M. Stoneking, F. Calafell, E. Sabid??, E. Bosch, Signatures of evolutionary adaptation in quantitative trait loci influencing trace element homeostasis in liver. *Molecular Biology and Evolution*. **33**, 738–754 (2016).
24. A. Roca-Umbert, R. Caro-Consuegra, D. Londono-Correa, G. F. Rodriguez-Lozano, R. Vicente, E. Bosch, Understanding signatures of positive natural selection in human zinc transporter genes. *Sci Rep*. **12**, 4320 (2022).
25. P. C. Sabeti, S. F. Schaffner, J. Lohmueller, P. Varilly, O. Shamovsky, A. Palma, T. S. Mikkelsen, D. Altshuler, E. S. Lander, Positive Natural Selection in the Human Lineage. *Science (1979)*. **312**, 1614–1620 (2006).
26. S. Casillas, R. Mulet, P. Villegas-Mirón, S. Hervas, E. Sanz, D. Velasco, J. Bertranpetit, H. Laayouni, A. Barbadilla, PopHuman: the human population genomics browser. *Nucleic Acids Research*. **46**, D1003–D1010 (2018).
27. M. Kircher, D. M. Witten, P. Jain, B. J. O 'roak, G. M. Cooper, J. Shendure, M. Edu, D. W. Edu, P. Org, A general framework for estimating the relative pathogenicity of human genetic variants. *Nat Genet*. **46**, 310–315 (2014).
28. L. Speidel, M. Forest, S. Shi, S. R. Myers, A method for genome-wide genealogy estimation for thousands of samples. *Nature Genetics*. **51**, 1321–1329 (2019).
29. B. M. Henn, L. L. Cavalli-Sforza, M. W. Feldman, The great human expansion. *Proceedings of the National Academy of Sciences*. **109**, 17758–17764 (2012).

30. S. R. Browning, B. L. Browning, Y. Zhou, S. Tucci, J. M. Akey, Analysis of Human Sequence Data Reveals Two Pulses of Archaic Denisovan Admixture. *Cell*. **173**, 53-61.e9 (2018).
31. S. Sankararaman, S. Mallick, N. Patterson, D. Reich, The Combined Landscape of Denisovan and Neanderthal Ancestry in Present-Day Humans. *Curr Biol*. **26**, 1241–7 (2016).
32. L. Skov, M. Coll Macià, G. Sveinbjörnsson, F. Mafessoni, E. A. Lucotte, M. S. Einarsdóttir, H. Jonsson, B. Halldorsson, D. F. Gudbjartsson, A. Helgason, M. H. Schierup, K. Stefansson, The nature of Neanderthal introgression revealed by 27,566 Icelandic genomes. *Nature*. **582**, 78–83 (2020).
33. G. Gower, P. I. Picazo, M. Fumagalli, F. Racimo, Detecting adaptive introgression in human evolution using convolutional neural networks. *Elife*. **10** (2021), doi:10.7554/eLife.64669.
34. M. J. Hubisz, A. L. Williams, A. Siepel, Mapping gene flow between ancient hominins through demography-aware inference of the ancestral recombination graph. *PLOS Genetics*. **16**, e1008895 (2020).
35. H. Rajeevan, U. Soundararajan, J. R. Kidd, A. J. Pakstis, K. K. Kidd, ALFRED: an allele frequency resource for research and teaching. *Nucleic Acids Research*. **40**, D1010–D1015 (2012).
36. D. J. Eide, Zinc transporters and the cellular trafficking of zinc. *Biochimica et Biophysica Acta*. **1763**, 711–722 (2006).
37. J. Xue, T. Xie, W. Zeng, Y. Jiang, X. C. Bai, Cryo-EM structures of human ZnT8 in both outward-and inward-facing conformations. *Elife*. **9**, 1–32 (2020).
38. J. Jumper, R. Evans, A. Pritzel, T. Green, M. Figurnov, O. Ronneberger, K. Tunyasuvunakool, R. Bates, A. Žídek, A. Potapenko, A. Bridgland, C. Meyer, S. A. A. Kohl, A. J. Ballard, A. Cowie, B. Romera-Paredes, S. Nikolov, R. Jain, J. Adler, T. Back, S. Petersen, D. Reiman, E. Clancy, M. Zielinski, M. Steinegger, M. Pacholska, T. Berghammer, S. Bodenstein, D. Silver, O. Vinyals, A. W. Senior, K. Kavukcuoglu, P. Kohli, D. Hassabis, Highly accurate protein structure prediction with AlphaFold. *Nature*. **596**, 583–589 (2021).
39. A. Kowalczyk, O. Gbadamosi, K. Kolor, J. Sosa, L. Andrzejczuk, G. Gibson, C. St Croix, M. Chikina, E. Aizenman, N. Clark, K. Kiselyov, Evolutionary rate covariation identifies SLC30A9 (ZnT9) as a mitochondrial zinc transporter. *Biochemical Journal*. **478**, 3205–3220 (2021).
40. K. Ishihara, T. Yamazaki, Y. Ishida, T. Suzuki, K. Oda, M. Nagao, Y. Yamaguchi-Iwai, T. Kambe, Zinc Transport Complexes Contribute to the Homeostatic Maintenance of Secretory Pathway Function in Vertebrate Cells. *Journal of Biological Chemistry*. **281**, 17743–17750 (2006).
41. T. Suzuki, K. Ishihara, H. Migaki, K. Ishihara, M. Nagao, Y. Yamaguchi-Iwai, T. Kambe, Two Different Zinc Transport Complexes of Cation Diffusion Facilitator Proteins Localized in the Secretory Pathway Operate to Activate Alkaline Phosphatases in Vertebrate Cells. *Journal of Biological Chemistry*. **280**, 30956–30962 (2005).
42. K. M. Taylor, S. Hiscox, R. I. Nicholson, C. Hogstrand, P. Kille, Protein kinase CK2 triggers cytosolic zinc signaling pathways by phosphorylation of zinc channel ZIP7. *Sci Signal*. **5** (2012), doi:10.1126/SCISIGNAL.2002585.
43. D. H. Fudge, R. Black, L. Son, K. Lejeune, Y. Qin, Optical Recording of Zn 2+ Dynamics in the Mitochondrial Matrix and Intermembrane Space with the GZnP2 Sensor. *ACS Chem Biol*. **13**, 1897–1905 (2018).

44. W. A. Prinz, A. Toulmay, T. Balla, The functional universe of membrane contact sites. *Nat Rev Mol Cell Biol*. **21**, 7–24 (2020).
45. Y. Perez, Z. Shorer, K. Liani-Leibson, P. Chabosseau, R. Kadir, M. Volodarsky, D. Halperin, S. Barber-Zucker, H. Shalev, R. Schreiber, L. Gradstein, E. Gurevich, R. Zarivach, G. A. Rutter, D. Landau, O. S. Birk, SLC30A9 mutation affecting intracellular zinc homeostasis causes a novel cerebro-renal syndrome. *Brain*. **140**, 928–939 (2017).
46. J. R. I. Coleman, H. A. Gaspar, J. Bryois, E. M. Byrne, A. J. Forstner, P. A. Holmans, C. A. de Leeuw, M. Mattheisen, A. McQuillin, J. M. Whitehead Pavlides, T. H. Pers, S. Ripke, E. A. Stahl, S. Steinberg, V. Trubetskoy, M. Trzaskowski, Y. Wang, L. Abbott, A. Abdellaoui, M. J. Adams, A. N. Adolfsson, E. Agerbo, H. Akil, D. Albani, N. Alliey-Rodriguez, T. D. Als, T. F. M. Andlauer, A. Anjorin, V. Antilla, S. van der Auwera, S. Awasthi, S.-A. Bacanu, J. A. Badner, M. Bækvad-Hansen, J. D. Barchas, N. Bass, M. Bauer, A. T. F. Beekman, R. Belliveau, S. E. Bergen, T. B. Bigdeli, E. B. Binder, E. Bøen, M. Boks, J. Boocock, M. Budde, W. Bunney, M. Burmeister, H. N. Buttenschøn, J. Bybjerg-Grauholm, W. Byerley, N. Cai, M. Casas, E. Castelao, F. Cerrato, P. Cervantes, K. Chambert, A. W. Charney, D. Chen, J. H. Christensen, C. Churchhouse, D. St Clair, T.-K. Clarke, L. Colodro-Conde, W. Coryell, B. Couvy-Duchesne, D. W. Craig, G. E. Crawford, C. Cruceanu, P. M. Czerski, A. M. Dale, G. Davies, I. J. Deary, F. Degenhardt, J. Del-Favero, J. R. DePaulo, E. M. Derks, N. Direk, S. Djurovic, A. L. Dobbyn, C. v. Dolan, A. Dumont, E. C. Dunn, T. C. Eley, T. Elvsåshagen, V. Escott-Price, C. C. Fan, H. K. Finucane, S. B. Fischer, M. Flickinger, J. C. Foo, T. M. Foroud, L. Forty, J. Frank, C. Fraser, N. B. Freimer, L. Frisén, K. Gade, D. Gage, J. Garnham, C. Giambartolomei, F. S. Goes, J. Goldstein, S. D. Gordon, K. Gordon-Smith, E. K. Green, M. J. Green, T. A. Greenwood, J. Grove, W. Guan, L. S. Hall, M. L. Hamshere, C. S. Hansen, T. F. Hansen, M. Hautzinger, U. Heilbronner, A. M. van Hemert, S. Herms, I. B. Hickie, M. Hipolito, P. Hoffmann, D. Holland, G. Homuth, C. Horn, J.-J. Hottenga, L. Huckins, M. Ising, S. Jamain, R. Jansen, J. S. Johnson, S. de Jong, E. Jorgenson, A. Juréus, R. Kandaswamy, R. Karlsson, J. L. Kennedy, F. F. Hassan Kiadeh, S. Kittel-Schneider, J. A. Knowles, M. Kogevinas, I. S. Kohane, A. C. Koller, J. Kraft, W. W. Kretzschmar, J. Krogh, R. Kupka, Z. Kutalik, C. Lavebratt, J. Lawrence, W. B. Lawson, M. Leber, P. H. Lee, S. E. Levy, J. Z. Li, Y. Li, P. A. Lind, C. Liu, L. M. Olde Loohuis, A. Maaser, D. J. MacIntyre, D. F. MacKinnon, P. B. Mahon, W. Maier, R. M. Maier, J. Marchini, L. Martinsson, H. Mbarek, S. McCarroll, P. McGrath, P. McGuffin, M. G. McInnis, J. D. McKay, H. Medeiros, S. E. Medland, D. Mehta, F. Meng, C. M. Middeldorp, E. Mihailov, Y. Milaneschi, L. Milani, S. S. Mirza, F. M. Mondimore, G. W. Montgomery, D. W. Morris, S. Mostafavi, T. W. Mühleisen, N. Mullins, M. Nauck, B. Ng, H. Nguyen, C. M. Nievergelt, M. G. Nivard, E. A. Nwulia, D. R. Nyholt, C. O'Donovan, P. F. O'Reilly, A. P. S. Ori, L. Oruc, U. Ösby, H. Oskarsson, J. N. Painter, J. G. Parra, C. B. Pedersen, M. G. Pedersen, A. Perry, R. E. Peterson, E. Pettersson, W. J. Peyrot, A. Pfennig, G. Pistis, S. M. Purcell, J. A. Quiroz, P. Qvist, E. J. Regeer, A. Reif, C. S. Reinbold, J. P. Rice, B. P. Riley, F. Rivas, M. Rivera, P. Roussos, D. M. Ruderfer, E. Ryu, C. Sánchez-Mora, A. F. Schatzberg, W. A. Scheftner, R. Schoevers, N. J. Schork, E. C. Schulte, T. Shehktman, L. Shen, J. Shi, P. D. Shilling, S. I. Shyn, E. Sigurdsson, C. Slaney, O. B. Smeland, J. H. Smit, D. J. Smith, J. L. Sobell, A. T. Spijker, M. Steffens, J. S. Strauss, F. Streit, J. Strohmaier, S. Szelinger, K. E. Tansey, H. Teismann, A. Teumer, R. C.

Thompson, W. Thompson, P. A. Thomson, T. E. Thorgeirsson, M. Traylor, J. Treutlein, A. G. Uitterlinden, D. Umbricht, H. Vedder, A. Viktorin, P. M. Visscher, W. Wang, S. J. Watson, B. T. Webb, C. S. Weickert, T. W. Weickert, S. M. Weinsheimer, J. Wellmann, G. Willemsen, S. H. Witt, Y. Wu, H. S. Xi, W. Xu, J. Yang, A. H. Young, P. Zandi, P. Zhang, F. Zhang, S. Zollner, R. Adolfsson, I. Agartz, M. Alda, V. Arolt, L. Backlund, B. T. Baune, F. Bellivier, K. Berger, W. H. Berrettini, J. M. Biernacka, D. H. R. Blackwood, M. Boehnke, D. I. Boomsma, A. Corvin, N. Craddock, M. J. Daly, U. Dannlowski, E. Domenici, K. Domschke, T. Esko, B. Etain, M. Frye, J. M. Fullerton, E. S. Gershon, E. J. C. de Geus, M. Gill, F. Goes, H. J. Grabe, M. Grigoroiu-Serbanescu, S. P. Hamilton, J. Hauser, C. Hayward, A. C. Heath, D. M. Hougaard, C. M. Hultman, I. Jones, L. A. Jones, R. S. Kahn, K. S. Kendler, G. Kirov, S. Kloiber, M. Landén, M. Leboyer, G. Lewis, Q. S. Li, J. Lissowska, S. Lucae, P. A. F. Madden, P. K. Magnusson, N. G. Martin, F. Mayoral, S. L. McElroy, A. M. McIntosh, F. J. McMahon, I. Melle, A. Metspalu, P. B. Mitchell, G. Morken, O. Mors, P. B. Mortensen, B. Müller-Myhsok, R. M. Myers, B. M. Neale, V. Nimgaonkar, M. Nordentoft, M. M. Nöthen, M. C. O'Donovan, K. J. Oedegaard, M. J. Owen, S. A. Paciga, C. Pato, M. T. Pato, N. L. Pedersen, B. W. J. H. Penninx, R. H. Perlis, D. J. Porteous, D. Posthuma, J. B. Potash, M. Preisig, J. A. Ramos-Quiroga, M. Ribasés, M. Rietschel, G. A. Rouleau, C. Schaefer, M. Schalling, P. R. Schofield, T. G. Schulze, A. Serretti, J. W. Smoller, H. Stefansson, K. Stefansson, E. Stordal, H. Tiemeier, G. Turecki, R. Uher, A. E. Vaaler, E. Vieta, J. B. Vincent, H. Völzke, M. M. Weissman, T. Werge, O. A. Andreassen, A. D. Børglum, S. Cichon, H. J. Edenberg, A. di Florio, J. Kelsoe, D. F. Levinson, C. M. Lewis, J. I. Nurnberger, R. A. Ophoff, L. J. Scott, P. Sklar, P. F. Sullivan, N. R. Wray, E. M. Byrne, A. J. Forstner, P. A. Holmans, C. A. de Leeuw, M. Mattheisen, A. McQuillin, J. M. Whitehead Pavlides, T. H. Pers, S. Ripke, E. A. Stahl, S. Steinberg, V. Trubetskoy, M. Trzaskowski, Y. Wang, L. Abbott, A. Abdellaoui, M. J. Adams, A. N. Adolfsson, E. Agerbo, H. Akil, D. Albani, N. Alliey-Rodriguez, T. D. Als, T. F. M. Andlauer, A. Anjorin, V. Antilla, S. van der Auwera, S. Awasthi, S.-A. Bacanu, J. A. Badner, M. Bækvad-Hansen, J. D. Barchas, N. Bass, M. Bauer, A. T. F. Beekman, R. Belliveau, S. E. Bergen, T. B. Bigdeli, E. B. Binder, E. Bøen, M. Boks, J. Boocock, M. Budde, W. Bunney, M. Burmeister, H. N. Buttenschøn, J. Bybjerg-Grauholm, W. Byerley, N. Cai, M. Casas, E. Castelao, F. Cerrato, P. Cervantes, K. Chambert, A. W. Charney, D. Chen, J. H. Christensen, C. Churchhouse, D. St Clair, T.-K. Clarke, L. Colodro-Conde, W. Coryell, B. Couvy-Duchesne, D. W. Craig, G. E. Crawford, C. Cruceanu, P. M. Czerski, A. M. Dale, G. Davies, I. J. Deary, F. Degenhardt, J. Del-Favero, J. R. DePaulo, E. M. Derks, N. Direk, S. Djurovic, A. L. Dobbyn, C. v. Dolan, A. Dumont, E. C. Dunn, T. C. Eley, T. Elvsåshagen, V. Escott-Price, C. C. Fan, H. K. Finucane, S. B. Fischer, M. Flickinger, J. C. Foo, T. M. Foroud, L. Forty, J. Frank, C. Fraser, N. B. Freimer, L. Frisén, K. Gade, D. Gage, J. Garnham, C. Giambartolomei, F. S. Goes, J. Goldstein, S. D. Gordon, K. Gordon-Smith, E. K. Green, M. J. Green, T. A. Greenwood, J. Grove, W. Guan, L. S. Hall, M. L. Hamshere, C. S. Hansen, T. F. Hansen, M. Hautzinger, U. Heilbronner, A. M. van Hemert, S. Herms, I. B. Hickie, M. Hipolito, P. Hoffmann, D. Holland, G. Homuth, C. Horn, J.-J. Hottenga, L. Huckins, M. Ising, S. Jamain, R. Jansen, J. S. Johnson, S. de Jong, E. Jorgenson, A. Juréus, R. Kandaswamy, R. Karlsson, J. L. Kennedy, F. F. Hassan Kiadeh, S. Kittel-Schneider, J. A. Knowles, M. Kogevinas, I. S. Kohane, A. C. Koller, J. Kraft, W.

W. Kretzschmar, J. Krogh, R. Kupka, Z. Kutalik, C. Lavebratt, J. Lawrence, W. B. Lawson, M. Leber, P. H. Lee, S. E. Levy, J. Z. Li, Y. Li, P. A. Lind, C. Liu, L. M. Olde Loohuis, A. Maaser, D. J. MacIntyre, D. F. MacKinnon, P. B. Mahon, W. Maier, R. M. Maier, J. Marchini, L. Martinsson, H. Mbarek, S. McCarroll, P. McGrath, P. McGuffin, M. G. McInnis, J. D. McKay, H. Medeiros, S. E. Medland, D. Mehta, F. Meng, C. M. Middeldorp, E. Mihailov, Y. Milaneschi, L. Milani, S. S. Mirza, F. M. Mondimore, G. W. Montgomery, D. W. Morris, S. Mostafavi, T. W. Mühleisen, N. Mullins, M. Nauck, B. Ng, H. Nguyen, C. M. Nievergelt, M. G. Nivard, E. A. Nwulia, D. R. Nyholt, C. O'Donovan, P. F. O'Reilly, A. P. S. Ori, L. Oruc, U. Ösby, H. Oskarsson, J. N. Painter, J. G. Parra, C. B. Pedersen, M. G. Pedersen, A. Perry, R. E. Peterson, E. Pettersson, W. J. Peyrot, A. Pfennig, G. Pistis, S. M. Purcell, J. A. Quiroz, P. Qvist, E. J. Regeer, A. Reif, C. S. Reinbold, J. P. Rice, B. P. Riley, F. Rivas, M. Rivera, P. Roussos, D. M. Ruderfer, E. Ryu, C. Sánchez-Mora, A. F. Schatzberg, W. A. Scheftner, R. Schoevers, N. J. Schork, E. C. Schulte, T. Shehktman, L. Shen, J. Shi, P. D. Shilling, S. I. Shyn, E. Sigurdsson, C. Slaney, O. B. Smeland, J. H. Smit, D. J. Smith, J. L. Sobell, A. T. Spijker, M. Steffens, J. S. Strauss, F. Streit, J. Strohmaier, S. Szelinger, K. E. Tansey, H. Teismann, A. Teumer, R. C. Thompson, W. Thompson, P. A. Thomson, T. E. Thorgeirsson, M. Traylor, J. Treutlein, A. G. Uitterlinden, D. Umbricht, H. Vedder, A. Viktorin, P. M. Visscher, W. Wang, S. J. Watson, B. T. Webb, C. S. Weickert, T. W. Weickert, S. M. Weinsheimer, J. Wellmann, G. Willemsen, S. H. Witt, Y. Wu, H. S. Xi, W. Xu, J. Yang, A. H. Young, P. Zandi, P. Zhang, F. Zhang, S. Zollner, R. Adolfsson, I. Agartz, M. Alda, V. Arolt, L. Backlund, B. T. Baune, F. Bellivier, K. Berger, W. H. Berrettini, J. M. Biernacka, D. H. R. Blackwood, M. Boehnke, D. I. Boomsma, A. Corvin, N. Craddock, M. J. Daly, U. Dannlowski, E. Domenici, K. Domschke, T. Esko, B. Etain, M. Frye, J. M. Fullerton, E. S. Gershon, E. J. C. de Geus, M. Gill, F. Goes, H. J. Grabe, M. Grigoroiu-Serbanescu, S. P. Hamilton, J. Hauser, C. Hayward, A. C. Heath, D. M. Hougaard, C. M. Hultman, I. Jones, L. A. Jones, R. S. Kahn, K. S. Kendler, G. Kirov, S. Kloiber, M. Landén, M. Leboyer, G. Lewis, Q. S. Li, J. Lissowska, S. Lucae, P. A. F. Madden, P. K. Magnusson, N. G. Martin, F. Mayoral, S. L. McElroy, A. M. McIntosh, F. J. McMahon, I. Melle, A. Metspalu, P. B. Mitchell, G. Morken, O. Mors, P. B. Mortensen, B. Müller-Myhsok, R. M. Myers, B. M. Neale, V. Nimgaonkar, M. Nordentoft, M. M. Nöthen, M. C. O'Donovan, K. J. Oedegaard, M. J. Owen, S. A. Paciga, C. Pato, M. T. Pato, N. L. Pedersen, B. W. J. H. Penninx, R. H. Perlis, D. J. Porteous, D. Posthuma, J. B. Potash, M. Preisig, J. A. Ramos-Quiroga, M. Ribasés, M. Rietschel, G. A. Rouleau, C. Schaefer, M. Schalling, P. R. Schofield, T. G. Schulze, A. Serretti, J. W. Smoller, H. Stefansson, K. Stefansson, E. Stordal, H. Tiemeier, G. Turecki, R. Uher, A. E. Vaaler, E. Vieta, J. B. Vincent, H. Völzke, M. M. Weissman, T. Werge, O. A. Andreassen, A. D. Børglum, S. Cichon, H. J. Edenberg, A. di Florio, J. Kelsoe, D. F. Levinson, C. M. Lewis, J. I. Nurnberger, R. A. Ophoff, L. J. Scott, P. Sklar, P. F. Sullivan, N. R. Wray, G. Breen, The Genetics of the Mood Disorder Spectrum: Genome-wide Association Analyses of More Than 185,000 Cases and 439,000 Controls. *Biological Psychiatry*. **88**, 169–184 (2020).

47. N. R. Wray, S. Ripke, M. Mattheisen, M. Trzaskowski, E. M. Byrne, A. Abdellaoui, M. J. Adams, E. Agerbo, T. M. Air, T. M. F. Andlauer, S.-A. Bacanu, M. Bækvad-Hansen, A. F. T. Beekman, T. B. Bigdeli, E. B. Binder, D. R. H. Blackwood, J. Bryois, H. N. Buttenschøn, J. Bybjerg-Grauholm, N. Cai, E.

Castelao, J. H. Christensen, T.-K. Clarke, J. I. R. Coleman, L. Colodro-Conde, B. Couvy-Duchesne, N. Craddock, G. E. Crawford, C. A. Crowley, H. S. Dashti, G. Davies, I. J. Deary, F. Degenhardt, E. M. Derks, N. Direk, C. v. Dolan, E. C. Dunn, T. C. Eley, N. Eriksson, V. Escott-Price, F. H. F. Kiadeh, H. K. Finucane, A. J. Forstner, J. Frank, H. A. Gaspar, M. Gill, P. Giusti-Rodríguez, F. S. Goes, S. D. Gordon, J. Grove, L. S. Hall, E. Hannon, C. S. Hansen, T. F. Hansen, S. Herms, I. B. Hickie, P. Hoffmann, G. Homuth, C. Horn, J.-J. Hottenga, D. M. Hougaard, M. Hu, C. L. Hyde, M. Ising, R. Jansen, F. Jin, E. Jorgenson, J. A. Knowles, I. S. Kohane, J. Kraft, W. W. Kretzschmar, J. Krogh, Z. Kutalik, J. M. Lane, Y. Li, Y. Li, P. A. Lind, X. Liu, L. Lu, D. J. MacIntyre, D. F. MacKinnon, R. M. Maier, W. Maier, J. Marchini, H. Mbarek, P. McGrath, P. McGuffin, S. E. Medland, D. Mehta, C. M. Middeldorp, E. Mihailov, Y. Milaneschi, L. Milani, J. Mill, F. M. Mondimore, G. W. Montgomery, S. Mostafavi, N. Mullins, M. Nauck, B. Ng, M. G. Nivard, D. R. Nyholt, P. F. O'Reilly, H. Oskarsson, M. J. Owen, J. N. Painter, C. B. Pedersen, M. G. Pedersen, R. E. Peterson, E. Pettersson, W. J. Peyrot, G. Pistis, D. Posthuma, S. M. Purcell, J. A. Quiroz, P. Qvist, J. P. Rice, B. P. Riley, M. Rivera, S. Saeed Mirza, R. Saxena, R. Schoevers, E. C. Schulte, L. Shen, J. Shi, S. I. Shyn, E. Sigurdsson, G. B. C. Sinnamon, J. H. Smit, D. J. Smith, H. Stefansson, S. Steinberg, C. A. Stockmeier, F. Streit, J. Strohmaier, K. E. Tansey, H. Teismann, A. Teumer, W. Thompson, P. A. Thomson, T. E. Thorgeirsson, C. Tian, M. Traylor, J. Treutlein, V. Trubetskoy, A. G. Uitterlinden, D. Umbricht, S. van der Auwera, A. M. van Hemert, A. Viktorin, P. M. Visscher, Y. Wang, B. T. Webb, S. M. Weinsheimer, J. Wellmann, G. Willemsen, S. H. Witt, Y. Wu, H. S. Xi, J. Yang, F. Zhang, V. Arolt, B. T. Baune, K. Berger, D. I. Boomsma, S. Cichon, U. Dannlowski, E. C. J. de Geus, J. R. DePaulo, E. Domenici, K. Domschke, T. Esko, H. J. Grabe, S. P. Hamilton, C. Hayward, A. C. Heath, D. A. Hinds, K. S. Kendler, S. Kloiber, G. Lewis, Q. S. Li, S. Lucae, P. F. A. Madden, P. K. Magnusson, N. G. Martin, A. M. McIntosh, A. Metspalu, O. Mors, P. B. Mortensen, B. Müller-Myhsok, M. Nordentoft, M. M. Nöthen, M. C. O'Donovan, S. A. Paciga, N. L. Pedersen, B. W. J. H. Penninx, R. H. Perlis, D. J. Porteous, J. B. Potash, M. Preisig, M. Rietschel, C. Schaefer, T. G. Schulze, J. W. Smoller, K. Stefansson, H. Tiemeier, R. Uher, H. Völzke, M. M. Weissman, T. Werge, A. R. Winslow, C. M. Lewis, D. F. Levinson, G. Breen, A. D. Børglum, P. F. Sullivan, Genome-wide association analyses identify 44 risk variants and refine the genetic architecture of major depression. *Nature Genetics*. **50**, 668–681 (2018).

48. G. Primes, M. Fieder, Real-life helping behaviours in North America: A genome-wide association approach. *PLOS ONE*. **13**, e0190950 (2018).
49. D. Nettle, The evolution of personality variation in humans and other animals. *Am Psychol*. **61**, 622–31 (2006).
50. A. Takeda, H. Fujii, T. Minamino, H. Tamano, Intracellular Zn(2+) signaling in cognition. *J Neurosci Res*. **92**, 819–24 (2014).
51. C. F. Gillespie, K. J. Ressler, Emotional learning and glutamate: translational perspectives. *CNS Spectr*. **10**, 831–9 (2005).
52. Y.-H. Kim, J.-W. Eom, J.-Y. Koh, Mechanism of Zinc Excitotoxicity: A Focus on AMPK. *Front Neurosci*. **14**, 577958 (2020).
53. R. S. Duman, G. Sanacora, J. H. Krystal, Altered Connectivity in Depression: GABA and Glutamate Neurotransmitter Deficits and Reversal by Novel Treatments. *Neuron*. **102**, 75–90 (2019).

54. T. McGrath, R. Baskerville, M. Rogero, L. Castell, Emerging Evidence for the Widespread Role of Glutamatergic Dysfunction in Neuropsychiatric Diseases. *Nutrients*. **14** (2022), doi:10.3390/nu14050917.
55. T. E. Daniels, E. M. Olsen, A. R. Tyrka, Stress and Psychiatric Disorders: The Role of Mitochondria. *Annu Rev Clin Psychol*. **16**, 165–186 (2020).
56. H. Manji, T. Kato, N. A. di Prospero, S. Ness, M. F. Beal, M. Krams, G. Chen, Impaired mitochondrial function in psychiatric disorders. *Nat Rev Neurosci*. **13**, 293–307 (2012).
57. L. Shao, M. v Martin, S. J. Watson, A. Schatzberg, H. Akil, R. M. Myers, E. G. Jones, W. E. Bunney, M. P. Vawter, Mitochondrial involvement in psychiatric disorders. *Ann Med*. **40**, 281–95 (2008).
58. I. Ionita-Laza, K. McCallum, B. Xu, J. D. Buxbaum, A spectral approach integrating functional genomic annotations for coding and noncoding variants. *Nature Publishing Group*. **48** (2016), doi:10.1038/ng.3477.
59. B. Gulko, M. J. Hubisz, I. Gronau, A. Siepel, A method for calculating probabilities of fitness consequences for point mutations across the human genome. *Nature Genetics*. **47**, 276–283 (2015).
60. A. Buniello, J. A. L. MacArthur, M. Cerezo, L. W. Harris, J. Hayhurst, C. Malangone, A. McMahon, J. Morales, E. Mountjoy, E. Sollis, D. Suveges, O. Vrousgou, P. L. Whetzel, R. Amode, J. A. Guillen, H. S. Riat, S. J. Trevanion, P. Hall, H. Junkins, P. Flicek, T. Burdett, L. A. Hindorff, F. Cunningham, H. Parkinson, The NHGRI-EBI GWAS Catalog of published genome-wide association studies, targeted arrays and summary statistics 2019. *Nucleic Acids Res*. **47**, D1005–D1012 (2019).
61. K. Watanabe, S. Stringer, O. Frei, M. Umićević Mirkov, C. de Leeuw, T. J. C. Polderman, S. van der Sluis, O. A. Andreassen, B. M. Neale, D. Posthuma, A global overview of pleiotropy and genetic architecture in complex traits. *Nat Genet*. **51**, 1339–1348 (2019).
62. D. Naon, M. Zaninello, M. Giacomello, T. Varanita, F. Grespi, S. Lakshminaranayan, A. Serafini, M. Semenzato, S. Herkenne, M. I. Hernández-Alvarez, A. Zorzano, D. de Stefani, G. W. Dorn, L. Scorrano, Critical reappraisal confirms that Mitofusin 2 is an endoplasmic reticulum–mitochondria tether. *Proceedings of the National Academy of Sciences*. **113**, 11249–11254 (2016).
63. Y. Qin, P. J. Dittmer, J. G. Park, K. B. Jansen, A. E. Palmer, J. S. Valentine, Measuring steady-state and dynamic endoplasmic reticulum and Golgi Zn 2þ with genetically encoded sensors. *Proceedings of the National Academy of Sciences*. **108**, 7351–7356 (2011).
64. F. Hahne, R. Ivanek, Visualizing Genomic Data Using Gviz and Bioconductor. *Methods in molecular biology*. **1418**, 335–351 (2016).
65. J. H. Marcus, J. Novembre, Visualizing the geography of genetic variants. *Bioinformatics*. **33**, 594–595 (2017).

## Acknowledgments

This work was supported by Agencia Estatal de Investigación (AEI) and Fondo Europeo de Desarrollo Regional (FEDER) (project grants PID2019-110933GB-I00/AEI/10.13039/501100011033, PID2019-106755RB-I00/AEI/10.13039/501100011033); Unidad de Excelencia María de Maeztu funded by the MCIN and the AEI (DOI:

10.13039/501100011033, Ref: CEX2018-000792-M); and by Direcció General de Recerca, Generalitat de Catalunya (2017SGR00702).

**Table 1.** Putative adaptive variants in the *SLC30A9* region.

| SNP | Ref | Alt | SNP type | AFR | EUR | EAS | SAS | AMR | CADD Phred score | eQTLs [a] (Tissue; NES; p-value) |
|---|---|---|---|---|---|---|---|---|---|---|
| rs2581434 | C | G | synonymous | 0.246 | 0.815 | 0.959 | 0.860 | 0.840 | 12.00 | Brain-Nucleus accumbens (basal ganglia); -0.23; 7.9 x $10^{-10}$ |
| rs1047626 | A | G | non-synonymous | 0.105 | 0.757 | 0.948 | 0.780 | 0.768 | 0.001 | Brain-Cortex; -0.24; 4.4 x $10^{-10}$ |
| rs2581452 | C | T | intronic | 0.193 | 0.776 | 0.958 | 0.800 | 0.803 | 11.38 | Brain-Nucleus accumbens (basal ganglia); -0.24; 2.5 x $10^{-11}$ |
| rs2660319 | G | A | intronic | 0.146 | 0.756 | 0.949 | 0.780 | 0.770 | 12.93 | Brain-Nucleus accumbens (basal ganglia); -0.22; 5.0 x $10^{-10}$ |
| rs1848182 | A | G | intronic | 0.193 | 0.776 | 0.958 | 0.800 | 0.803 | 10.10 | Brain-Nucleus accumbens (basal ganglia); -0.24; 2.5 x $10^{-11}$ |
| rs2581424 | G | A | intronic | 0.188 | 0.776 | 0.958 | 0.800 | 0.804 | 10.78 | Brain-Nucleus accumbens (basal ganglia); -0.23; 3.1 x $10^{-10}$ |
| rs15857 | C | A | synonymous | 0.188 | 0.776 | 0.958 | 0.800 | 0.804 | 14.93 | Brain-Nucleus accumbens (basal ganglia); -0.23; 3.1 x $10^{-10}$ |
| rs7439806 | G | A | intronic | 0.188 | 0.776 | 0.958 | 0.800 | 0.804 | 10.63 | Brain-Nucleus accumbens (basal ganglia); -0.23; 3.1 x $10^{-10}$ |
| rs55835604 | T | A | intronic | 0.191 | 0.776 | 0.958 | 0.800 | 0.804 | 13.81 | Brain-Nucleus accumbens (basal ganglia); -0.23; 3.1 x $10^{-10}$ |
| rs12510574 | G | A | intronic | 0.393 | 0.123 | 0.037 | 0.100 | 0.134 | 12.13 | Adipose - Subcutaneous; -0.16; 1.9 x $10^{-6}$ |
| rs4861014 | A | G | intronic | 0.067 | 0.752 | 0.951 | 0.780 | 0.759 | 12.23 | Brain-Nucleus accumbens (basal ganglia); -0.25; 1.2 x $10^{-12}$ |
| rs10019356 | A | G | intronic | 0.176 | 0.789 | 0.960 | 0.820 | 0.811 | 15.41 | Brain-Nucleus accumbens (basal ganglia); -0.24; 4.2 x $10^{-10}$ |
| rs7660223 | C | T | intronic | 0.153 | 0.789 | 0.960 | 0.820 | 0.808 | 15.33 | Brain-Nucleus accumbens (basal ganglia); -0.24; 4.2 x $10^{-10}$ |
| rs11051 | G | A | 3' UTR | 0.051 | 0.751 | 0.951 | 0.780 | 0.758 | 10.81 | Brain-Nucleus accumbens (basal ganglia); -0.25; 1.2 x $10^{-12}$ |
| rs11935648 | G | A | 3' UTR | 0.176 | 0.788 | 0.960 | 0.820 | 0.808 | 1.44 | Brain-Nucleus accumbens (basal ganglia); -0.24; 4.2 x $10^{-10}$ |
| rs12511999 | C | T | 3' UTR | 0.087 | 0.751 | 0.951 | 0.780 | 0.764 | 0.24 | Brain-Nucleus accumbens (basal ganglia); -0.26; 9.9 x $10^{-14}$ |
| rs10938178 | G | C | 3' UTR | 0.067 | 0.751 | 0.951 | 0.780 | 0.759 | 1.32 | Brain-Nucleus accumbens (basal ganglia); -0.25; 1.2 x $10^{-12}$ |
| rs12512101 | C | T | 3' UTR | 0.086 | 0.751 | 0.951 | 0.780 | 0.764 | 4.31 | Brain-Nucleus accumbens (basal ganglia); -0.26; 9.9 x $10^{-14}$ |

[a] eQTLs described for *SLC30A9*. Extracted from GTEx database V7. NES: Normalized effect size.

**Figure Legends**

**Figure 1. Signals of positive selection and putative adaptive variants at *SLC30A9*.** (A) Signatures of adaptation in the *SLC30A9* region. Chromosomal location and genes located along the *SLC30A9* flanking region are displayed at the top. In the first selection panel, window-based $F_{ST}$ values when comparing CEU versus YRI and CHB versus YRI are represented by cyan and pink bars, respectively. Similarly, window-based Fay and Wu's H values and XP-EHH scores (using YRI as the reference population) in CEU and CHB are shown with the same color scheme in the middle and bottom selection panels, respectively. Overlapping population scores can result in purple shades. Horizontal cyan and pink lines represent the genomic average of each test for each population, whereas 2 standard deviations are represented by the background shade in each case as a mean to interpret the genome-wide significance of each selection signature. All selection score test values were extracted from the corresponding 1000 Genomes Project populations as available at the PopHuman browser (http://pophuman.uab.cat) (*26*) and represented using the Gviz package (*64*). (B) Allele frequencies at rs1047626 and rs4861157 across human populations in the 1000 Genomes Project. Frequency plots were downloaded from the Geography of Genetic Variants Browser (https://popgen.uchicago.edu/ggv/) (*65*). (C) Allele frequency trajectories and selection coefficients inferred with CLUES for rs1047626 in CHB and CEU and for rs4861157 in YRI. (D) Schematic representation of the two major human haplotypes as defined by 170 SNPs in high linkage disequilibrium ($r^2$>0.8) with rs1047626 in CEU and CHB and the corresponding allele states found in the Denisovan and Neanderthal genomes from the UCSC Genome Browser (GRCh37/hg19). Derived states are indicated in black, ancestral alleles in grey, and genomic positions without coverage in the Neanderthal genome in white. Den to Papuan and Den to Melanesian represent Denisovan introgression segments previously described in Melanesians (*33*) and Papua New Guineans (*34*). The black and grey arrows point to the rs1047626 and rs4861157 positions. GWAS hits are indicated with an asterisk (see Supplementary Table S2 for details). (E) Sharing of human archaic alleles in Non-African populations. In red, divergent alleles between the indicated branches in the phylogeny; in black, shared alleles; in blue, shared alleles with Neanderthals; in green, shared alleles with the Denisovan genome. Within parenthesis, number of shared derived alleles. (F) Differential *SLC30A9* expression in the substantia nigra according to the rs1047626 and rs4861157 genotypes as available at the GTEX portal (https://www.gtexportal.org/home/). NES, normalized effect sizes.

**Figure 2.** Characterization of the structure and overexpression of ZnT9 in HEK293 cells. (A) ZnT9 protein structure prediction by AlphaFold, showing 6 transmembrane domains and a cytosolic N-terminus, where the Met50Val substitution is indicated by a red arrow. (B) Protein sequence of the ZnT9 transporter with the Met50Val substitution in red and the predicted alpha-helices corresponding to transmembrane domains in blue. (C) Representative Western blot against HA and GAPDH in cells transfected with ZnT9-50Met, ZnT9-50Val, or an empty vector. (D) Representative pictures of the membrane and intracellular immunostaining of HEK293 cells expressing ZnT9-50Met and ZnT9-50Val isoforms (both in green). Nucleae were stained with DAPI (blue). Scale bar = 10 µm.

**Figure 3. Subcellular localization of ZnT9 variants.** (A) Superresolution STED microscopy in cells transfected with ZnT9-50Met and ZnT9-50Val immunoassayed with anti-HA (green) and with the mitochondrial marker anti-TOM20. Scale bar = 10 µm. (B-C) Bar graph representing mean inter-mitochondrial distance (B) and relative mitochondria area (C) in cells transfected with ZnT9-50Met or ZnT9-50Val (n=10). *** $p<0.001$ using Bonferroni test between conditions. (D) Bar graph measuring FRET between the endoplasmic reticulum and mitochondria transfected with an empty vector (control), ZnT9-50Met or ZnT9-50Val together with the FEMP probe (n=46-65).

**Figure 4. Characterization of the impact on cellular zinc homeostasis of ZnT9 variant overexpression in HEK293 cells.** (A) RT-PCR comparing the expression of several ZTs in basal conditions in cells transfected with ZnT9-50Met, ZnT9-50Val, or an empty vector. $2^{-(DDCT)}$ plotted using GAPDH as the housekeeping gene (ZIP1, ZIP6, and ZIP7 n = 6; Rest of ZTs n = 3); * $p<0.05$ versus control using Bonferroni, # $p<0.05$ versus control using t-test. (B) Evaluation of zinc content by flow cytometry using Zinquin in 10 µM and 100 µM of $ZnSO_4$ (n = 9); *** $p<0.001$ using t-test. (C) Evaluation of endoplasmic zinc content using an endoplasmic reticulum fluorescent zinc sensor (ER-ZapCY1) in basal and 100 µM $ZnSO_4$ conditions (n = 14-20). *** $p<0.001$ using t-test; * $p<0.05$ using Mann-Whitney test. (D) RT-PCR comparing the expression of several ZnT transporters in basal conditions in cells transfected with ZnT9-50Met, ZnT9-50Val, or an empty vector. $2^{-(DDCT)}$ plotted using GAPDH as the housekeeping gene (n = 5-6) ** $p<0.01$, *** $p<0.001$ using Bonferroni. (E) Evaluation of endoplasmic zinc content using an ER fluorescent zinc sensor (ER-ZapCY1) in basal and 100 µM $ZnSO_4$ in the presence of DMSO and Zip7 blocker (n = 12-19). (F) Evaluation of zinc mitochondrial intermembrane space content using SMAC-Gn2Zn probe in conditions of 10 µM

and 100 µM $ZnSO_4$ (n = 8-9); # $p<0.05$ using t-test between transfection conditions. (G) Evaluation of zinc mitochondrial matrix content using Mito-cCherry-Gn2Zn incubating 40min with basal and 100 µM $ZnSO_4$ conditions (n = 9-12); ** $p<0.01$ using t-test between basal and 100 µM zinc conditions, # $p<0.05$ using t-test between transfection conditions. (H) Viability MTT assay in cells transfected with ZnT9-50Met, ZnT9-50Val, or an empty vector incubated for 24h at 0, basal and 100 µM $ZnSO_4$ conditions (n=8-15) * $p<0.05$, ** $p<0.01$ using Bonferroni between transfection conditions, # $p<0.05$ using Bonferroni between zinc conditions.

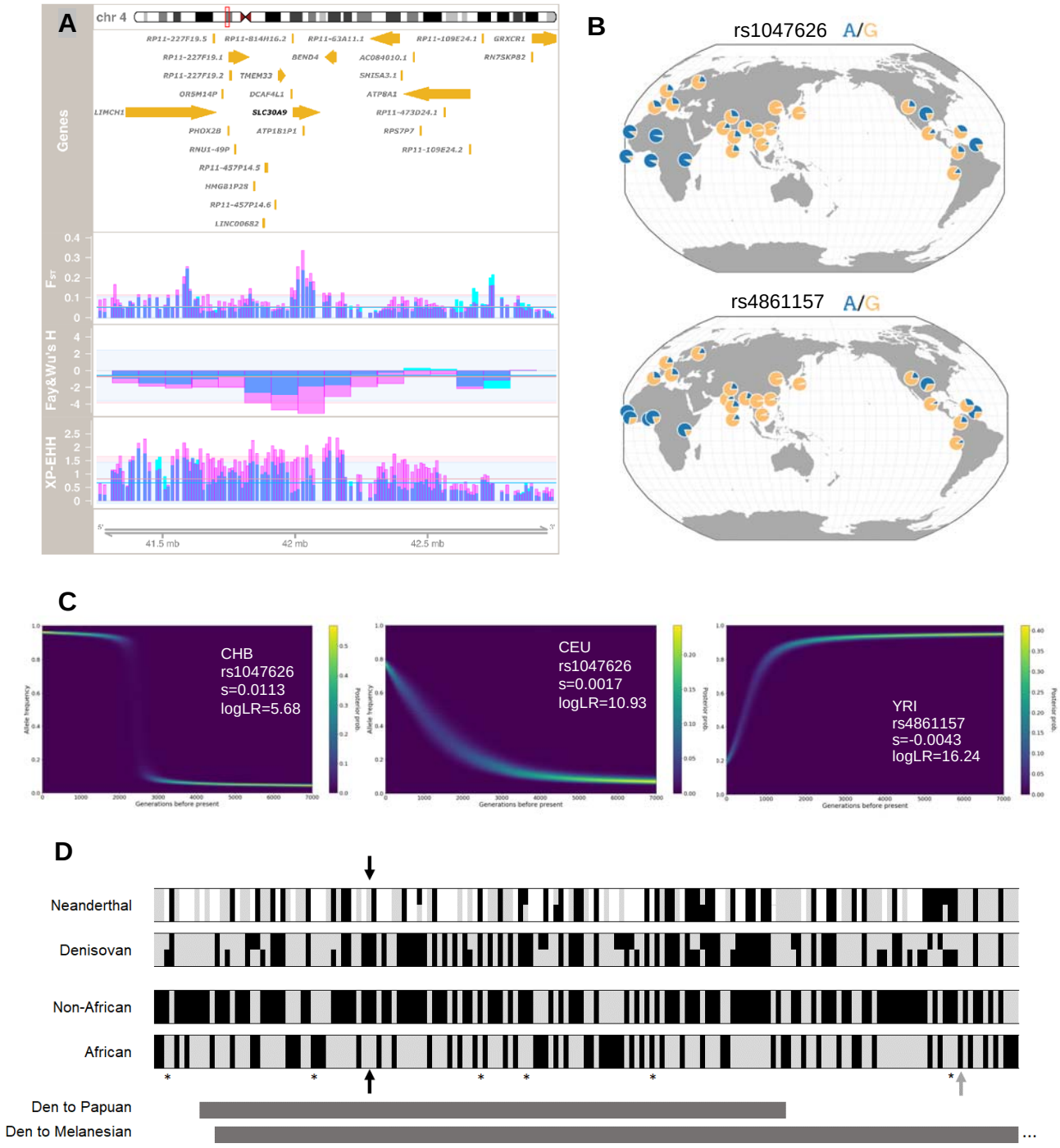
A
chr 4
Genes
RP11-227F19.5
RP11-814H16.2
RP11-63A11.1
RP11-109E24.1
GRXCR1
RP11-227F19.1
BEND4
AC084010.1
RN7SKP82
RP11-227F19.2
TMEM33
SHISA3.1
OR5M14P
DCAF4L1
ATP8A1
LIMCH1
SLC30A9
RP11-473D24.1
PHOX2B
ATP1B1P1
RPS7P7
RNU1-49P
RP11-109E24.2
RP11-457P14.5
HMGB1P28
RP11-457P14.6
LINC00682
FST
Fay&Wu's H
XP-EHH
41.5 mb
42 mb
42.5 mb
B
rs1047626 A/G
rs4861157 A/G
C
CHB
rs1047626
s=0.0113
logLR=5.68
CEU
rs1047626
s=0.0017
logLR=10.93
YRI
rs4861157
s=-0.0043
logLR=16.24
Generations before present
D
Neanderthal
Denisovan
Non-African
African
Den to Papuan
Den to Melanesian
E
6 Mya
600 kya
400 kya
100 kya
50 kya
Present
14
96
(46)
40
70
(44)
32
139
(79)
164
7(4)
Neand
Den
Non-African
African
Chimpanzee
F
SLC30A9
rs1047626
Brain - Substantia nigra
SLC30A9
rs4861157
Brain - Substantia nigra
Norm. Expression
AA
(17)
AG
(33)
GG
(84)
p-value = 1.5E-8
NES = -0.39
AA
(14)
AG
(33)
GG
(67)
p-value = 2.2E-9
NES = -0.42

**Figure 1**

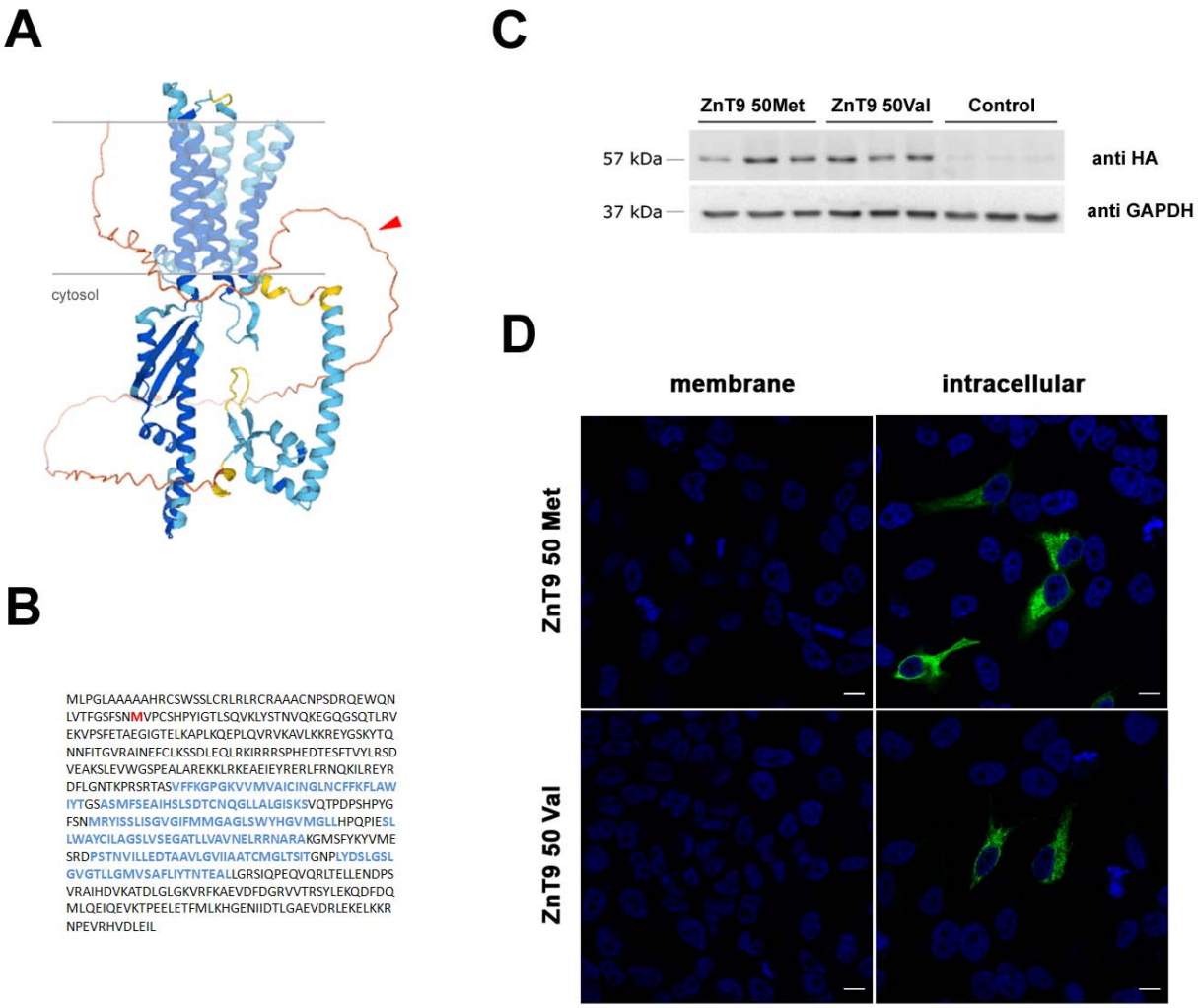
A
cytosol
B
MLPGLAAAAAHRCSWSSLCRLRLRCRAAACNPSDRQEWQN
LVTFGSFSNMVPCSHPYIGTLSQVKLYSTNVQKEGQGSQTLRV
EKVPSFETAEGIGTELKAPLKQEPLQVRVKAVLKKREYGSKYTQ
NNFITGVRAINEFCLKSSDLEQLRKIRRRSPHEDTESFTVYLRSD
VEAKSLEVWGSPEALAREKKLRKEAEIEYRERLFRNQKILREYR
DFLGNTKPRSRTASVFFKGPGKVVMVAICINGLNCFFKFLAW
IYTGSASMFSEAIHSLSDTCNQGLLALGISKSVQTPDPSHPYG
FSNMRYISSLISGVGIFMMGAGLSWYHGVMGLLHPQPIESL
LWAYCILAGSLVSEGATLLVAVNELRRNARAKGMSFYKYVME
SRDPSTNVILLEDTAAVLGVIIAATCMGLTSITGNPLYDSLGSL
GVGTLLGMVSAFLIYTNTEALLGRSIQPEQVQRLTELLENDPS
VRAIHDVKATDLGLGKVRFKAEVDFDGRVVTRSYLEKQDFDQ
MLQEIQEVKTPEELETFMLKHGENIIDTLGAEVDRLEKELKKR
NPEVRHVDLEIL
C
ZnT9 50Met
ZnT9 50Val
Control
57 kDa
37 kDa
anti HA
anti GAPDH
D
membrane
intracellular
ZnT9 50 Met
ZnT9 50 Val

**Figure 2**

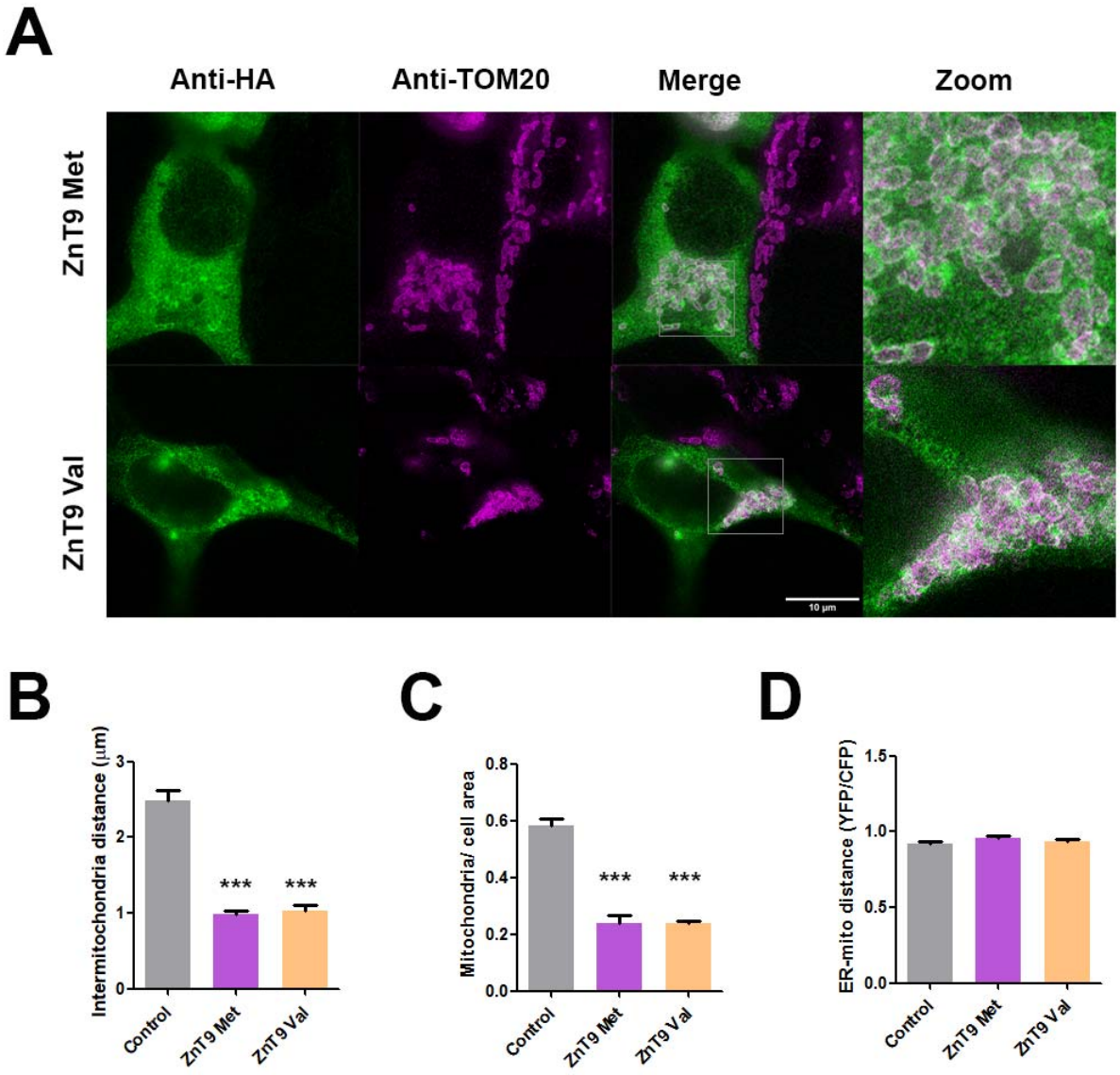
A
Anti-HA
Anti-TOM20
Merge
Zoom
ZnT9 Met
ZnT9 Val
10 µm
B
Intermitochondria distance (µm)
3
2
1
0
***
***
Control
ZnT9 Met
ZnT9 Val
C
Mitochondria/ cell area
0.8
0.6
0.4
0.2
0.0
***
***
Control
ZnT9 Met
ZnT9 Val
D
ER-mito distance (YFP/CFP)
1.5
1.0
0.5
0.0
Control
ZnT9 Met
ZnT9 Val

**Figure 3**

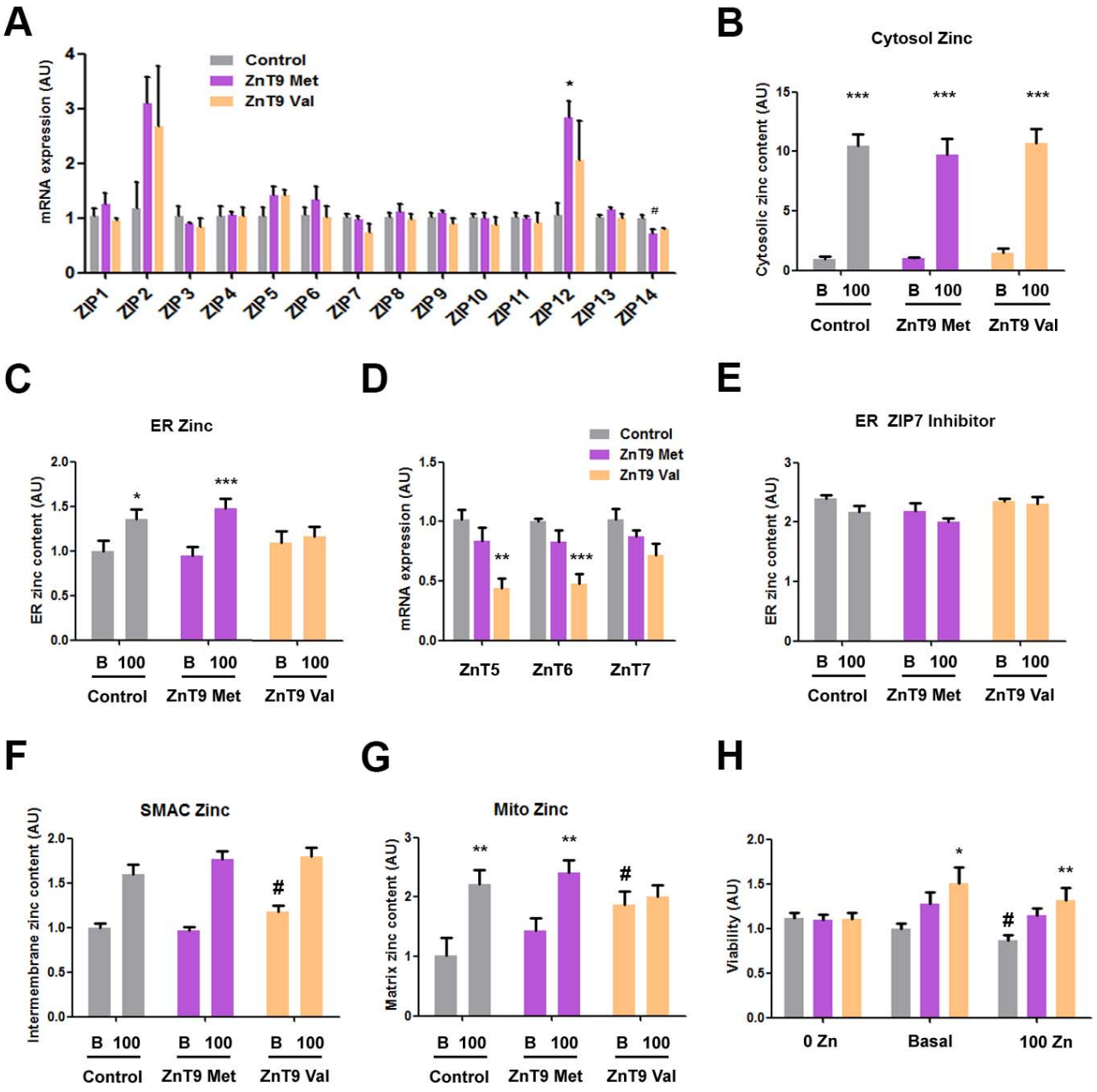
A
mRNA expression (AU)
Control
ZnT9 Met
ZnT9 Val
ZIP1
ZIP2
ZIP3
ZIP4
ZIP5
ZIP6
ZIP7
ZIP8
ZIP9
ZIP10
ZIP11
ZIP12
ZIP13
ZIP14
B
Cytosol Zinc
Cytosolic zinc content (AU)
B 100
Control
ZnT9 Met
ZnT9 Val
C
ER Zinc
ER zinc content (AU)
D
mRNA expression (AU)
ZnT5
ZnT6
ZnT7
E
ER ZIP7 Inhibitor
ER zinc content (AU)
F
SMAC Zinc
Intermembrane zinc content (AU)
G
Mito Zinc
Matrix zinc content (AU)
H
Viability (AU)
0 Zn
Basal
100 Zn

**Figure 4**